Use of Fiber Reinforced Concrete in Bridge Approach Slabs

Final Report

Deflection Softening FRC

Deflection Hardening HyFRC

Use of Fiber Reinforced Concrete in Bridge Approach Slabs

Final Report

Report No. CA09-0632

December 2008

Prepared By:

Civil and Environmental Engineering Department
University of California, Berkeley
Berkeley, CA 94720

Prepared For:

California Department of Transportation
Engineering Services Center
1801 30th Street
Sacramento, CA 95816

California Department of Transportation
Division of Research and Innovation, MS-83
1227 O Street
Sacramento, CA 95814

DISCLAIMER STATEMENT

STATE OF CALIFORNIA DEPARTMENT OF TRANSPORTATION
TECHNICAL REPORT DOCUMENTATION PAGE
TR0003 (REV. 10/98)

1. REPORT NUMBER	2. GOVERNMENT ASSOCIATION NUMBER	3. RECIPIENT'S CATALOG NUMBER
CA09-0632		

4. TITLE AND SUBTITLE	5. REPORT DATE
Use of Fiber Reinforced Concrete in Bridge Approach Slabs	December, 2008
	6. PERFORMING ORGANIZATION CODE

7. AUTHOR(S)	8. PERFORMING ORGANIZATION REPORT NO.
C.P. Ostertag, and J. Blunt	

9. PERFORMING ORGANIZATION NAME AND ADDRESS	10. WORK UNIT NUMBER
Civil and Environmental Engineering Department University of California, Berkeley Berkeley, CA 94720	11. CONTRACT OR GRANT NUMBER DRI Research Task No. 0632 Contract No. 65A0201

12. SPONSORING AGENCY AND ADDRESS	13. TYPE OF REPORT AND PERIOD COVERED
California Department of Transportation Engineering Services Center 1801 30th Street Sacramento, CA 95816 California Department of Transportation Division of Research and Innovation, MS-83 1227 O Street Sacramento, CA 95814	Final Report
	14. SPONSORING AGENCY CODE 913

15. SUPPLEMENTAL NOTES

16. ABSTRACT

Bridge approach slabs are deteriorating at a much faster rate than expected resulting in a massive need for repairs and premature replacement costing millions of dollars annually. Both environmental and traffic loading causes the concrete to worsen which accelerates the deterioration process by allowing deleterious agents to enter the concrete. In order to enhance the service life of bridge approach slabs the material needs to comply with certain performance criteria such as crack resistance, durability enhancement and post crack flexural stiffness. A Hybrid Fiber Reinforced Concrete (HyFRC) was developed for the use in bridge approach slabs in Area III jurisdiction which are exposed to severe environmental conditions. Deflection hardening was used as a performance goal in the design of the HyFRC composite.

The research program consisted of four parts. First (1), a performance based materials approach to bridge approach slabs was developed. The fiber reinforced composite was designed to exhibit deflection hardening through an average measure of ductility exceeding the yield strain of steel rebar (i.e. > 0.002). Four point flexure tests on 6 in. (152 mm) deep beam specimens were conducted in order to quantify the material flexure performance. Second (2), the existing California Department of Transportation (Caltrans) bridge approach slab design was used as the basis for element sizing and reinforcement ratios. Four-point flexure tests (1/2 scale models of an existing bridge approach slabs) were conducted and HyFRC beams were compared against plain concrete control beams with and without conventional steel reinforcement. Third (3), an extensive durability study was conducted on how the crack resistance provided by the HyFRC mitigates durability problems associated with frost action and corrosion. The bridge approach slab is highly susceptible to deterioration from freeze-thaw cycling and reinforcement corrosion due to the anticipated location (i.e. Area III jurisdiction). Compared to the plain concrete specimens the HyFRC exhibited improved performance in regards to both freeze/thaw resistance and scaling resistance. To study the effect of cracking/crack resistance on corrosion behavior, cyclic flexure tests were conducted on reinforced beam elements composed of HyFRC and a comparable plain concrete in order to induce surface cracking. For a specified load demand in excess of the plain concrete f_r and below the yield strength of the rebar, the HyFRC flexural specimens showed a high propensity for crack resistance (no surface cracks were visible as opposed to the reinforced plain concrete). Corrosion behavior was then monitored by ponding salt solution on the cracked surface and higher corrosion rates i_{corr} (measured by polarization resistance) by nearly 1 order magnitude were observed in the reinforced plain concrete specimens. The observed increased corrosion rates were confirmed by direct gravimetric analysis of the bars after removal. The study concludes (4) with a discussion of how the observed improvements in flexural performance in the presence of the fibers can be used for a new design detail for bridge approach slabs.

17. KEY WORDS	18. DISTRIBUTION STATEMENT
Bridge approach slabs, fiber reinforced concrete composites, stiffness, performance based materials approach, durability studies, corrosion, frost resistance, scaling, flexural performance of ½ scale bridge approach slab.	No restrictions. This document is available to the public through the National Technical Information Service, Springfield, VA 22161

19. SECURITY CLASSIFICATION (of this report)	20. NUMBER OF PAGES	21. PRICE
Unclassified	95 Pages	

Reproduction of completed page authorized

Final Report

<u>Use of Fiber Reinforced Concrete in Bridge Approach Slabs</u>

C. P. Ostertag and J. Blunt
UC Berkeley Civil and Environmental Engineering Department

Technical Report Documentation Page

1. Report No. CA09-0632	2. Government Accession No.	3. Recipient's Catalog No.
4. Title and Subtitle Use of Fiber Reinforced Concrete in Bridge Approach Slabs		5. Report Date June 2008
		6. Performing Organization Code
7. Author(s) C.P. Ostertag and J. Blunt		8. Performing Organization Report No.
9. Performing Organization Name and Address Civil & Environmental Engineering Department University of California Berkeley, CA 94720		10. Work Unit No. (TRAIS)
		11. Contract or Grant No.
12. Sponsoring Agency Name and Address California Department of Transportation Sacramento, CA 95814		13. Type of Report and Period Covered Final Report, 5/1/2005-6/30/2008
		14. Sponsoring Agency Code

15. Supplementary Notes

This study was sponsored by the California Department of Transportation (Caltrans)

16. Abstract

Bridge approach slabs are deteriorating at a much faster rate than expected resulting in a massive need for repairs and premature replacement costing millions of dollars annually. Both environmental and traffic loading causes the concrete to worsen which accelerates the deterioration process by allowing deleterious agents to enter the concrete. In order to enhance the service life of bridge approach slabs the material needs to comply with certain performance criteria such as crack resistance, durability enhancement and post crack flexural stiffness. A Hybrid Fiber Reinforced Concrete (HyFRC) was developed for the use in bridge approach slabs in Area III jurisdiction which are exposed to severe environmental conditions. Deflection hardening was used as a performance goal in the design of the HyFRC composite.

The research program consisted of four parts. First (1), a performance based materials approach to bridge approach slabs was developed. The fiber reinforced composite was designed to exhibit deflection hardening through an average measure of ductility exceeding the yield strain of steel rebar (i.e. > 0.002). Four point flexure tests on 6 in. (152 mm) deep beam specimens were conducted in order to quantify the material flexure performance. Second (2), the existing California Department of Transportation (CalTrans) bridge approach slab design was used as the basis for element sizing and reinforcement ratios. Four-point flexure tests (1/2 scale models of an existing bridge approach slabs) were conducted and HyFRC beams were compared against plain concrete control beams with and without conventional steel reinforcement. Third (3), an extensive durability study was conducted on how the crack resistance provided by the HyFRC mitigates durability problems associated with frost action and corrosion. The bridge approach slab is highly susceptible to deterioration from freeze-thaw cycling and reinforcement corrosion due to the anticipated location (i.e. Area III jurisdiction). Compared to the plain concrete specimens the HyFRC exhibited improved performance in regards to both freeze/thaw resistance and scaling resistance. To study the effect of cracking/crack resistance on corrosion behavior, cyclic flexure tests were conducted on reinforced beam elements composed of HyFRC and a comparable plain concrete in order to induce surface cracking. For a specified load demand in excess of the plain concrete f_r and below the yield strength of the rebar, the HyFRC flexural specimens showed a high propensity for crack resistance (no surface cracks were visible as opposed to the reinforced plain concrete). Corrosion behavior was then monitored by ponding salt solution on the cracked surface and higher corrosion rates i_{corr} (measured by polarization resistance) by nearly 1 order magnitude were observed in the reinforced plain concrete specimens. The observed increased corrosion rates were confirmed by direct gravimetric analysis of the bars after removal. The study concludes (4) with a discussion of how the observed improvements in flexural performance in the presence of the fibers can be used for a new design detail for bridge approach slabs.

17. Key Word Bridge approach slabs, fiber reinforced concrete composites, stiffness, performance based materials approach, durability studies, corrosion, frost resistance, scaling, flexural performance of ½ scale bridge approach slab,		18. Distribution Statement	
19. Security Classif. (of this report) Unclassified	20. Security Classif. (of this page) Unclassified	21. No. of Pages 91	22. Price

Form DOT F 1700.7 (8-72)   Reproduction of completed page authorized

EXECUTIVE SUMMARY

Bridge approach slabs are deteriorating at a much faster rate than predicted, resulting in a massive need of repairs and premature replacements. To enhance the service life of bridge approach slabs the concrete material needs to comply with certain performance criteria such as crack resistance due to mechanical and environmental conditions and post-crack flexural stiffness. A Hybrid Fiber Reinforced Concrete (HyFRC) was developed for the use of bridge approach slabs in Area III jurisdiction which are exposed to severe environmental conditions. Deflection hardening was used as a performance goal in the design of the HyFRC composite. The plain concrete matrix modulus of rupture was sustained through a ductility demand equivalent to the yield strain of conventional steel rebar in order to enhance the crack resistance associated with mechanical loading condition as well as environmental conditions.

Monotonic flexure tests were carried out for both un-reinforced and reinforced specimens (with conventional steel rebars) consisting of plain concrete and the HyFRC. The existing CalTrans bridge approach slab design was used as the basis for element sizing and reinforcing ratios. Increases in ultimate flexural strength when using the HyFRC were approximately 200% in the un-reinforced concrete elements, while increases in the HyFRC flexural yield strength were 90% in the reinforced elements. Furthermore, the HyFRC increased both the post crack flexural stiffness and flexural strength with section reinforcing ratios as high as 1.1% relative to the plain concrete element.

The anticipated application for the HyFRC material is as bridge approach slab located in an Area III jurisdiction. Hence the bridge approach slab is highly susceptible to deterioration from freeze-thaw cycling and reinforcement corrosion. Plain concrete is examined relative to HyFRC under a series of accelerated durability tests in order to determine the impacts of the proposed hybrid fiber gradation on corrosion and freeze-thaw related deterioration mechanisms. Compared to the plain concrete specimens the HyFRC exhibited improved performance in regards to both freeze/thaw resistance and scaling resistance. To study the effect of cracking/crack resistance on corrosion behavior, cyclic flexure tests were conducted on reinforced beam elements composed of HyFRC and a comparable plain concrete in order to induce surface cracking. For a specified load demand in excess of the plain concrete f_r and below the yield strength of the rebar, the HyFRC flexural specimens showed a high propensity for crack resistance (no surface cracks were visible as opposed to the reinforced plain concrete). Corrosion behavior was then monitored by ponding salt solution on the cracked surface and higher corrosion rates i_{corr} (measured by polarization resistance) by nearly 1 order magnitude were observed in the reinforced plain concrete specimens. The observed increased corrosion rates were confirmed by direct gravimetric analysis of the bars after removal. Chloride concentration measurements validated the differentiation in corrosion rate between the specimens with larger amounts of Cl⁻ measured in the reinforced plain concrete. This demonstrated that the crack resisting characteristics of the HyFRC influenced the time dependent nature of i_{corr} by slowing the rate of Cl⁻ ingress.

Further experimentation on uncracked cylindrical specimens showed that differentiation between the reinforced plain concrete and reinforced HyFRC corrosion rates were negligible through the period of observation. However, investigations with accelerated specimens demonstrated a delayed impact of the HyFRC. This occurred when the level of corrosion was sufficient enough to produce cracking that caused an increase in the corrosion rate in the plain concrete specimen. The increased corrosion rate was attributed to reduced resistance to ionic conductivity in a cracked matrix.

The improved mechanical performance due to HyFRC may have implications for the design of certain structural elements (such as section or rebar reduction). It is anticipated that performance increases (i.e. increased crack resistance, flexural stiffness and strength) will be observed when the HyFRC is used in place of plain concrete, however the exact magnitude should be verified with full scale testing. In the case of element redesign (i.e. section or rebar reduction) full scale testing is highly recommended.

CONTENTS

ILLUSTRATION AND TABLES

DISCLAIMER

The contents of this report reflect the views of the authors who are responsible for the facts and the accuracy of the data presented herein. The contents do no necessarily reflect the official views or policies of the STATE OF CALIFORNIA. This report does not constitute a standard, specification, or regulation.

ACKNOWLEDGMENTS

1 INTRODUCTION

Bridge approach slabs provide a transitional roadway between pavement and the bridge superstructure. This transition is crucial in reducing the dynamic effects imposed on the bridge by traffic and truckloads. It is also an ideal test-bed for durability related studies because it has been shown that a number of factors can significantly reduce the service life of the element (Timmerman 1976, Seo et al. 2002, White et al. 2005).

1.1 Problems with current bridge approach slabs

Bridge approach slabs are deteriorating at a much faster rate than expected resulting in a massive need for repairs and premature replacement costing millions of dollars annually. Many approach slabs have exhibited severe cracking from the effect of heavy impact loads, coupled with unknown or inadequate soil conditions (e.g., settlement, embankment bulging, poor fill material, inadequate compaction, poor drainage, etc.), and durability problems associated with frost action and corrosion. These cracks occur even on relatively newly constructed slabs. Various design schemes of the approach and transition slabs (e.g. alteration of the thickness of the approach slab, adding number of rebar, increasing concrete strength, etc.) have been implemented, however, the cracking has persisted.

1.2 Objectives and Scope

Both environmental and traffic loading causes the concrete to worsen which accelerates the deterioration process by allowing deleterious agents to enter the concrete. In order to enhance the service life of bridge approach slabs the material needs to comply with certain performance criteria such as crack resistance, durability enhancement and post crack flexural stiffness.

The strategy developed by this study was to consider a holistic approach to element design (from the material level to element geometry and reinforcing layout). This was done in order to provide more degrees of freedom that could be used to optimize performance and increase service life. A hybrid fiber reinforced (HyFRC) composite was chosen as the study material. The rationale behind the use of a HyFRC based mix can be referred to as Deterioration Reduction through Micro- and Macrocrack Control, or the DRMC approach. Micro and macrofibers are used simultaneously to control the micro and macrocracks, respectively. The microfibers delay microcrack initiation and propagation and the macrofibers reduce macrocrack propagation.

1.3 Overview of Report Contents

The results of this research program are presented in four parts. First (1), a performance based materials approach to bridge approach slabs was developed. This section includes the materials performance criteria, the mechanical performance objectives and the optimization processes that were involved in order for the HyFRC to meet these performance goals. Four point flexure tests on 6 in. (152 mm) deep beam specimens were

conducted in order to quantify the material flexure performance. Second (2), the existing California Department of Transportation (CalTrans) bridge approach slab design was used as the basis for element sizing and reinforcement ratios. Four-point flexure tests (1/2 scale models of an existing bridge approach slabs) were conducted and HyFRC beams were compared against plain concrete control beams with and without conventional steel reinforcement. Following this (3) an extensive durability study was conducted on how the crack resistance provided by hybrid fiber reinforcement affects corrosion related durability problems of embedded rebar. Validation studies of the material freeze-thaw behavior were also conducted. Preliminary results (4) of an investigation on how the HyFRC consistency can be improved to the point of self consolidation are provided and the study concludes (5) with a discussion of how the observed improvements in flexural performance in the presence of the fibers can be used for a new design detail for bridge approach slabs.

2 PERFORMANCE BASED MATERIALS APPROACH TO BRIDGE APPROACH SLABS

2.1 Materials Performance Criteria and Mechanical Performance Objectives

It was anticipated that fiber hybridization would provide an efficient mechanism for i) crack resistance however, in order to enhance the service life of bridge approach slabs and facilitate the ease of material placement, other performance goals needed to be addressed that included ii) cracked flexural stiffness, iii) surface wear resistance and iv) workability.

i) Crack resistance is one of the primary demands on concrete based material performance. Cracking in reinforced concrete slab elements can be from a number of mechanisms that include plastic and drying shrinkage, frost action, corrosion and traffic loading (Kyle 2001). From the standpoint of corrosion resistance, these cracks allow deleterious compounds to enter the concrete, thereby accelerating corrosion related deterioration processes. One way to reduce deterioration is by making the concrete highly impermeable to prevent these aggressive agents from infiltrating the concrete. Hence both CalTrans (CalTrans 2003) as well as ACI (ACI 318 2002) recommend a w/c ratio of 0.4. However, for a structure to have a high degree of durability (and a corresponding increase in service life), low permeability is a necessary but not sufficient condition. Resistance to cracking is equally important.

Since cracks initiate as microcracks, they need to be influenced at this stage, prior to becoming macrocracks. One effective way to enhance the resistance to crack propagation is through fiber reinforcements. However, conventional fibers are not well suited to bridge and influence these small microcracks at onset because their diameters are too large and the fibers are spaced too far apart in conventional FRCs (Fig.1a). To influence these microcracks, microfibers were utilized. Not only are their diameters much smaller (10-40μm compared to 500μm of conventional macrofibers), their numerical density (number of fibers per area of any cross section) will be much higher for microfibers than it is for macrofibers for identical fiber volume fractions (Fig. 1b)). Once microcracks become macrocracks, they need to be bridged by macro fibers to resist further propagation and crack opening. Hence, a HyFRC based matrix appears to be an effective means to resist crack propagation.
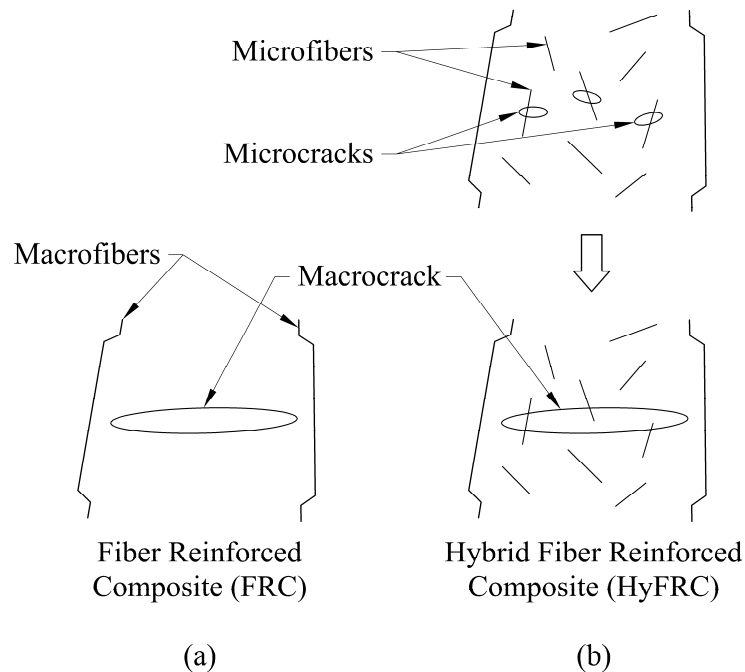
Fig. 1. – Schematic representation of fiber spacing and characteristic cracking in (a) FRC and (b) HyFRC

ii) Post crack flexural stiffness is necessary to prevent excessive deflection of bridge approach slabs after soil erosion. In order to retain stiffness, the HyFRC composite needs to delay macrocrack formation and exhibit deflection hardening. However, the enhanced matrix strength due to the low w/c ratio of 0.4 at a low fiber volume fraction, typically used in conventional FRC's, is more likely to promote the formation of a localized crack system which is characterized by a lower toughness, fiber pull-out and a single, large width crack (Li and Wu 1992, Tjiptobroto and Hansen 1993). Banthia and Trottier (1995) showed that in terms of flexural response, this is most commonly characterized by load instability immediately following macrocrack formation in the matrix. It is also apparent that for any load demands in excess of the matrix cracking strength, the onset of crack localization results in reduced stiffness. This is schematically shown in Fig. 2. In this case, given a conventional fiber reinforced matrix of one type of fiber and a HyFRC at the same total fiber volume fraction V_f, a load demand P in excess of the first crack strength will produce a deflection Δ_{FRC} and Δ_{HyFRC} in the FRC and the HyFRC composite respectively. Elimination of the load instability results in a condition where Δ_{HyFRC} will always be less than Δ_{FRC}. The HyFRC composite needs to be designed such that it eliminates the instability and increases the composite strength following the matrix first crack strength. It is important to note that hardening is anticipated only under a flexural stress distribution. This behavior does not imply a hardening response in direct tension.
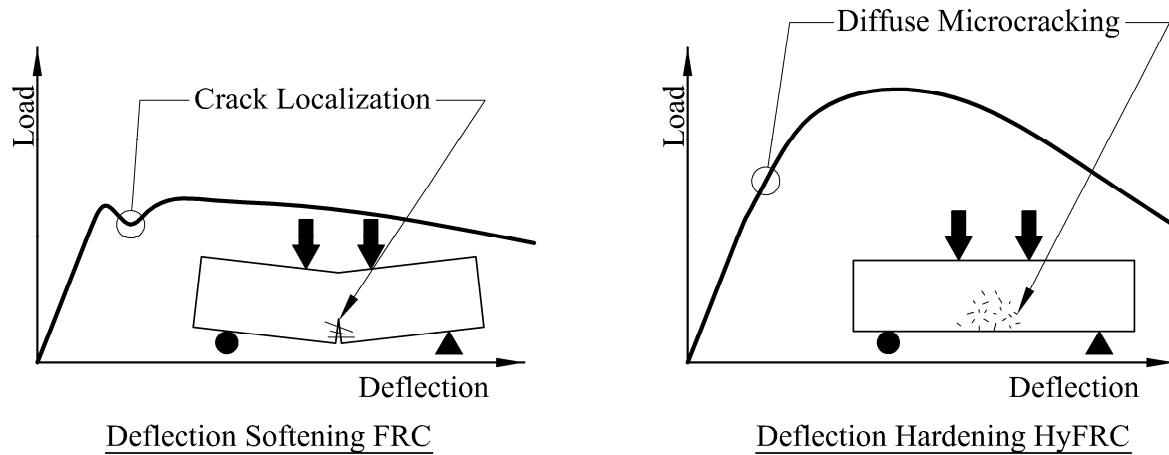
Fig. 2 – Comparison between deflection softening and deflection hardening

Incorporation of stiff aggregates into the mix design can significantly enhance the composite elastic modulus. Furthermore, due to the fact that the HyFRC will be used to completely replace the existing concrete used for bridge approach slabs, any reductions in the elastic modulus of the composite will negatively affect the material's deflection resistance. Numerous cement based composites have already been developed that show significant deflection hardening behavior, however none utilize coarse aggregates and some require non-conventional placing and curing techniques, which impedes their full scale use in cast-in-place applications (Rossi 2001). Mortar based matrices facilitate incorporation of higher fiber volume fractions by enhancing material consistency as well as reducing the degree of fiber balling, which is attributed to the presence of large coarse aggregates (Mangat and Swamy 1974a,b). However, it was the goal of this study to rely on conventional materials and processing methods while minimizing the total fiber volume fraction in order facilitate the ease of material use in field applications.

iii) Surface wear resistance requires the incorporation of coarse aggregates as well. Aggregates are typically the harder phase of a plain concrete composite. Unless the w/c

7

is reduced to levels on the order of 0.30, it is expected that the mortar phase will wear much more rapidly than a coarse aggregate of intermediate hardness (Laplante et al. 1991). Bridge approach slabs and bridge deck slabs are typically exposed elements where their surface is expected to act as the primary wear surface. Coarse aggregates are necessary in order to provide a hard, wear resistant surface for a prolonged service life.

A moderate degree of _iv) workability_ is required for cast in place applications such as bridge approach slabs. Large fiber volume fractions of a single fiber type can result in improved material performance, especially if the fibers are long and have high aspect ratios (Naaman 2003). However, it is understood that fibers of this nature incorporated at high dosages cannot be used with a conventional concrete matrix without significantly affecting the material homogeneity and consistency. Fiber hybridization provides an alternative by allowing reductions in total fiber content while maintaining mechanical performance and promoting a higher degree of material consistency. The relative proportions of fibers used in a HyFRC can be modified in order to reach a targeted degree of flexural performance, while the constitutive proportions of the concrete based matrix (i.e. cement paste, fine aggregate and coarse aggregate content) can be optimized in order to maximize material consistency.

In terms of mechanical performance criteria for the HyFRC mix design, controlled ductility was preferred over high strength. In reinforced concrete design, it is understood that the tensile strain capacity of concrete is an order of magnitude smaller than the yield strain capacity of the conventional steel reinforcement. Load-deflection response of reinforced concrete is typically characterized by linear elastic behavior up to concrete

first crack, at which point load can continue to be increased, but at a reduced stiffness. It is within this region of reduced stiffness that cracks open and grow through fatigue cycling. The goal was to design a material that maintained deflection hardening characteristics through an average measure of ductility equivalent to the yield strain of steel (~0.002 for Gr. 60). This was done to ensure that the cover concrete would not be compromised by cracking through the extreme load case and corresponding ductility demand where the conventional steel reinforcement reaches its yield point.

A performance criteria associated with the yield strain of rebar is an effective benchmark for the design of a HyFRC composite. However, it is very difficult to use strain alone as a performance criterion. This arises from the fact that the discrete nature of crack formation and resulting failure in plain concrete makes experimentally determined values of strain heavily dependent on the specimen size and monitoring method. Hence, a numerically based computational approach was employed to determine the expected flexural performance of the HyFRC composite in four point bending. The modeling method consisted of combining elastic beam flexure with a layered non-linear hinge based on fictitious crack propagation. The model was robust enough so that the width of the nonlinear hinge Lf could be varied as well as the position of the hinge relative to the centerline of the beam. This is shown in Fig. 3.
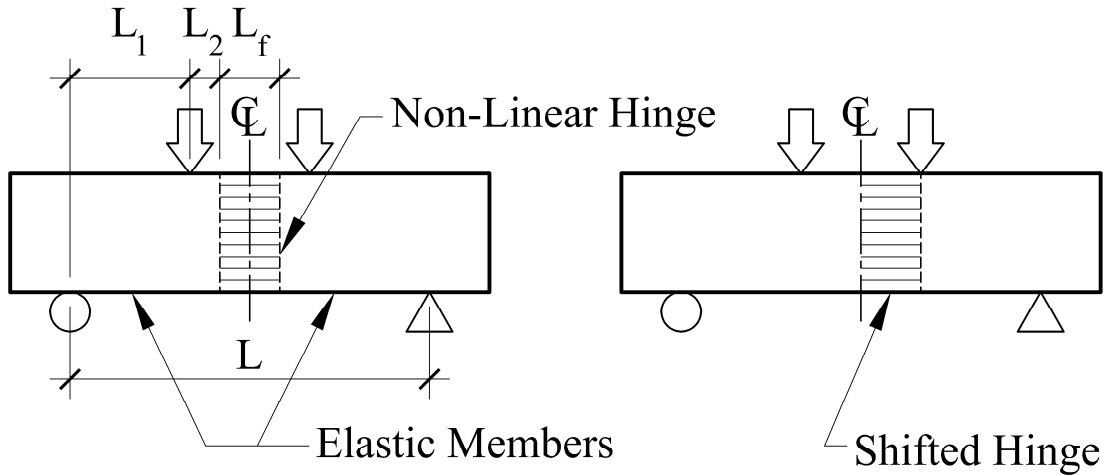
Fig 3: Modeling Method

Flexure load-deformation behavior was determined by incrementing the hinge rotation and then numerically solving for a compatible stress distribution. In the hinge region an Euler-Bernoulli compatibility assumption was used while a Timoshenko type shear deformation relationship was incorporated in the elastic regions to account for the deep beam proportions. The cracked portion of the hinge was approximated with a bilinear stress-crack width σ-w relationship with slopes m_1 and m_2. Parameters for defining the nonlinear constitutive behavior are shown in Figs. 4 & 5.
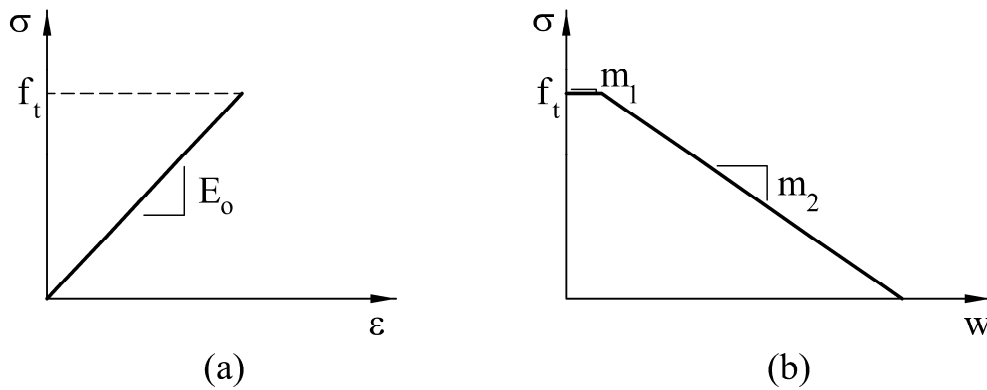
Fig. 4: Proposed Constitutive Parameters for (a) Elastic Tensile σ-ε Behavior
and (b) Cracked Tensile σ-w Behavior
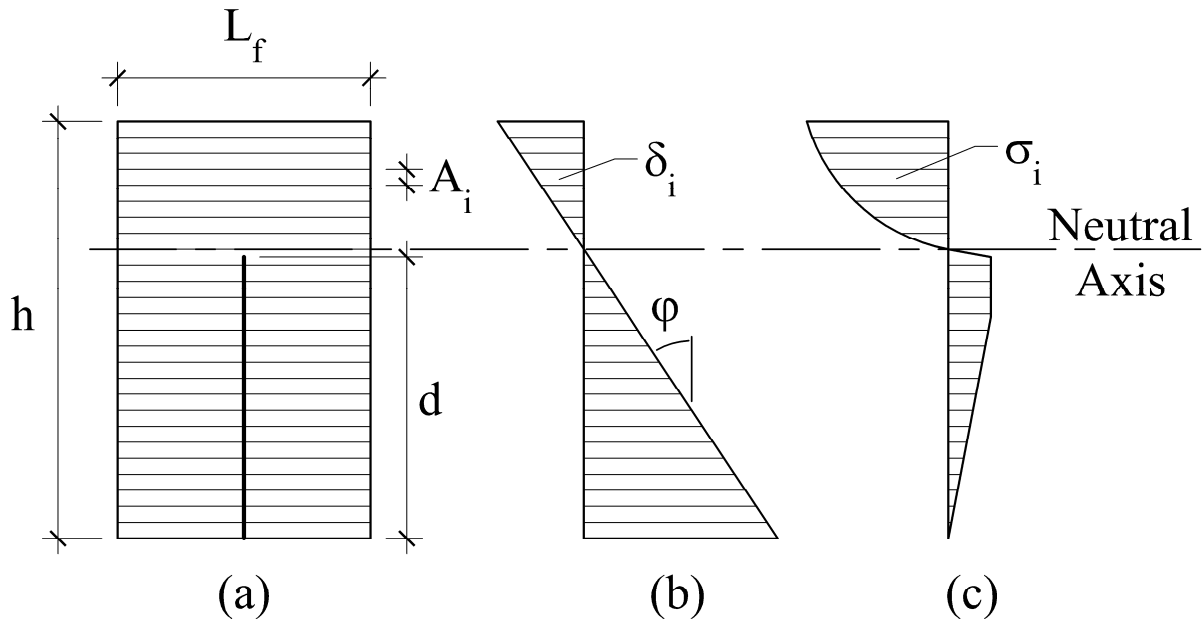
Fig. 5: Schematic Representation of (a) Hinge Discretization, (b) Assumed Section Rotational Displacement and (c) Stress Distributions

2.2 Constitutive Materials and HyFRC Mix Design

Three types of fiber with different sizes and material composition were used. Table 1 summarizes the pertinent characteristics of the fibers. Polyvinyl Alcohol (PVA) fibers were chosen for the micro level and steel fibers were chosen for the macro. The PVA fibers have the benefit of high stiffness, when compared to a stiffness of 725 ksi (5 GPa) typical of polypropylene and polyethylene fibers (ACI 544.1R-96 1997). Also, the hydrophilic nature of the PVA promotes a strong chemical bond with the surrounding cement paste matrix (Li et al. 2001). Steel fibers were chosen for crack resistance at the macrolevel because of their high stiffness and hooked end. The hooked end provides mechanical anchorage through which the fiber stiffness can be fully developed.

11

Table 1. – Fiber properties

Designation	Material	Length in. (mm)	Diameter in. (mm)	Strength ksi (MPa)	Stiffness ksi (GPa)
PA	PVA	0.32 (8)	0.0016 (0.04)	230 (1600)	6090 (42)
S1	Steel, Hooked	1.18 (30)	0.0217 (0.55)	160 (1100)	29000 (200)
S2	Steel, Hooked	2.36 (60)	0.0295 (0.75)	150 (1050)	29000 (200)

With regards to the matrix composition, two types of aggregate were used during the trial batching process. They consisted of a 1 in. (25.4 mm) maximum sized rounded river gravel and a 3/8 in. (9.5 mm) maximum sized pea gravel. The fine aggregate was a coarse sand (fineness modulus = 3.2) and an ASTM C150 Type II cement was used as the binder. The admixture suite consisted of a polycarboxylate superplasticizer and a compatible air entraining agent. When entrained air was needed, air contents for the mixes were adjusted to 5-8%, measured by ASTM C138. Air entraining was specified early in the project because of typical performance demands associated with an Area III application. The anticipation that freezing conditions can be expected for the material meant that mixes with air entraining had to be developed and tested.

All specimens were prepared using a planetary mixer, consolidated under external vibration and wet cured for 7 days followed by 21 days of dry curing in ambient lab conditions before testing. The aggressive curing regime was used to simulate field curing of a concrete bridge approach slab. Two different concrete based matrix types were employed during trial batching as well. This was done in order to provide a comparable matrix from the standpoint of compression strength and cement paste volume, when air-

12

entraining was or was not used. Relative mix proportions can be found in Table 2. The

CONC1 matrix was proportioned in accordance with CalTrans specifications for a

corrosive environment (w/c = 0.4, cement content = 475 kg/m^3 max), such that the

inclusion of the fibers could be compared against an existing methodology for plain

concrete mix proportioning. Plain concrete control mixtures were proportioned for

comparison against an equivalent HyFRC such that the fiber content replaced an

equivalent volume of coarse aggregate. When specified, the conventional reinforcing bar

steel (rebar) used for the reinforced elements was an ASTM A615 grade 60.

Table 2 - Weight ratios of matrix types

Designation	Type	Cement	Water	CA	FA
CONC1[a,b]	Concrete	1.0	0.4	1.64	1.71
CONC2	Concrete	1.0	0.54	1.54	2.00

[a] 0.02% air entraining (solid content per cement weight) required for plain concrete mix
[b] 0.005% air entraining and 0.08% superplasticizer required for HyFRC mix

2.3 Flexure Test Method

It was understood that the typical service level demands on a bridge approach slab

consisted of flexural loading; therefore material performance was to be characterized in

terms of its flexural behavior. The test apparatus consisted of a 4 point bending jig with

pin and roller type supports. Both the load jig and support system allowed for out-of-

plane rotation in order to eliminate torsional effects due to minor imperfections in

specimen orthogonality. Specimen size was 6 x 6 x 24 in. (150 x 150 x 600 mm) with a

clear span of 18 in. (450 mm). This is illustrated in Fig. 6. Flexure tests were carried out

per ASTM C1609, using displacement control with a servo controlled, closed loop

system. A bending yoke was used in order to isolate actual beam displacements from

extraneous displacements associated with support settlement and stiffness of the test apparatus. The bending yoke was anchored at the support points along the beam neutral axis. A Linear Variable Differential Transformer (LVDT) was attached to the yoke on both sides of the beam. The average displacement between the two LVDT's was used as the measure of the beam centerline displacement.
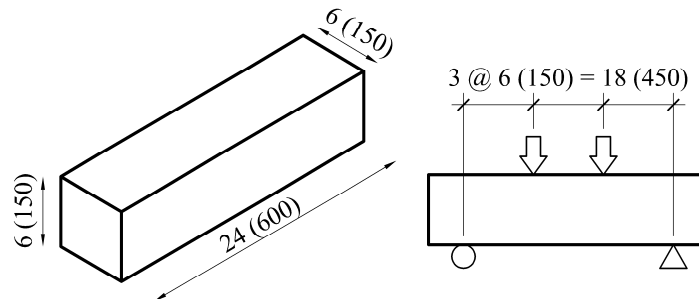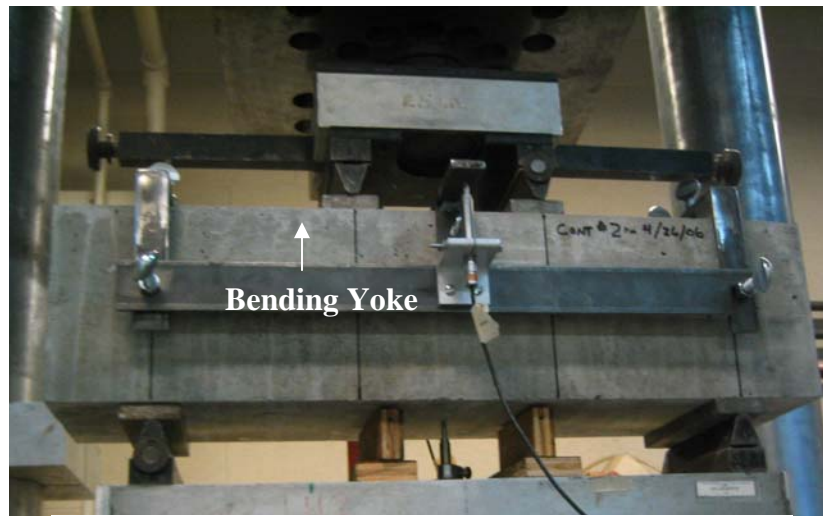
Fig. 6 – Four point flexure test setup [in. (mm)]

The proposed setup was used for an extensive series of trial batch flexure tests where the fiber gradation was modified and the flexural performance was characterized. Deflection hardening up to the yield strain of the reinforcing bar (i.e. 0.002) was the target performance goal and various fiber reinforcing trial batch flexure specimens were rated against this target performance goal. The trial batch fiber proportions are provided in

14

Table 3 and their flexural behavior is plotted in Fig. 7. Fiber reinforced concrete mixes with flexural peak loads falling in the region denoted "Very Likely" met the deflection hardening performance goal. Data falling in the region of "Unlikely" did not meet the performance goal.

Table 3 - Trial batch fiber proportions

Trial Batch	Max. Agg. Size [in. (mm)]	Fiber Volume Fraction [%]		
		PA	S1	S2[a]
F1	1 (25)	--	--	0.7
F2	1 (25)	0.3	--	0.7
F3	1 (25)	0.3	--	0.7
F4	3/8 (9.5)	0.2	0.5	0.5
F5	3/8 (9.5)	0.2	0.5	0.8

[a]aspect ratio (length/diameter) of fiber for mixes F1 & F2 = 65, aspect ratio for mixes F3, F4 &F5 = 80
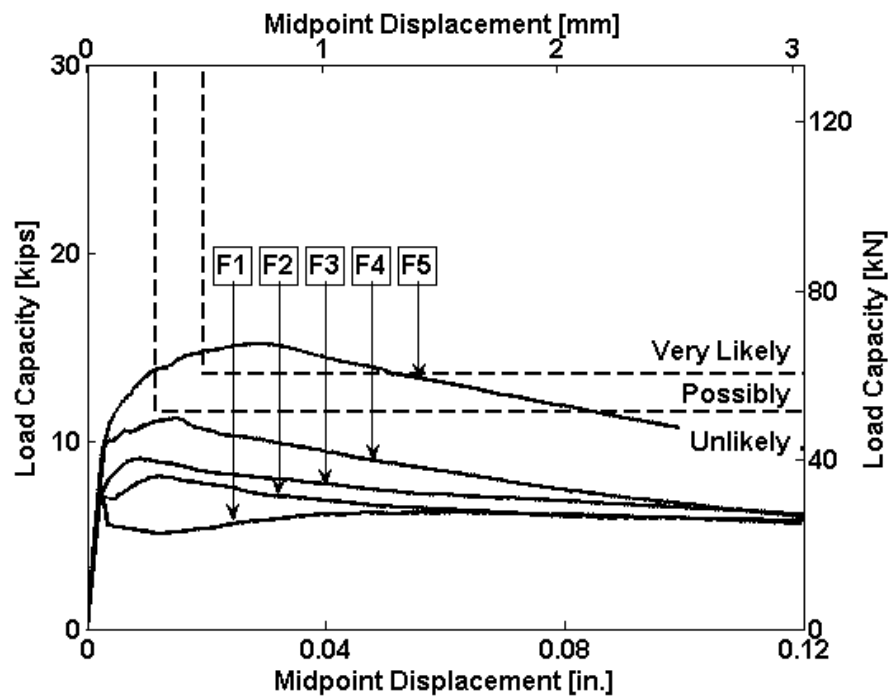
Fig. 7 – Trial batch flexural behavior plotted against the strain based deflection hardening performance goals (CONC1 matrix w/ air = 5-8%)

15

The method applied to the trial batch procedure was to approach the performance goal from below, by gradually increasing fiber content such that the goal was met with the minimum amount of fibers. General guidelines concerning the effect of fiber size on the mechanical performance of fiber reinforced elements have been determined by others (Rossi et al. 1987, Cheyrezy et al. 1995) however fiber effect on the mix workability was a larger driving force behind the relative fiber proportioning. The propensity of the S2 fibers to clump during mixing forced limiting their V_f to below 1%. The hydrophilic behavior of the PA type fibers limited their concentrations to low levels because their adsorptive capacity significantly increased the water demand. The trial batch F5 was the fiber gradation that met the deflection hardening performance goals, so it was used for subsequent testing and analysis.

2.4 Optimum Consistency Verification

With an acceptable fiber gradation determined from trial batch flexure tests, the aggregate phase of the matrix was modified in order to explore its impact on the overall consistency. This was necessary because the aggregate gradation for the trial batch flexure tests was based on recommendations in the literature for steel fiber FRC (Rossi and Harrouche 1990). In the presence of a hybrid fiber gradation it became necessary to verify the applicability of the proposed gradation.

A method for FRC consistency optimization, proposed by Rossi and Harrouche (1990), was applied to HyFRC mix proportion optimization. The method requires that one

16

assume fibers affect the consistency of the concrete on the same level as the aggregate and that the most workable mix is the one that has the densest packing of the sand, gravel and fiber phases. Once the fiber proportions were determined the fine aggregate to coarse aggregate (sand to gravel) weight ratio could be varied and consistency measured through the use of a workabilimeter. The workabilimeter used by Rossi and Harrouche used an external vibrating apparatus which was attached to a box and could vibrate 0.04 yd^3 (30 L) of concrete. It is noted that this is a particularly robust means to measure the consistency of fiber reinforced and other stiff concrete based mixes. The use of an electric or pneumatic based external vibrator allows it to be easily adapted for field use. Due to constraints associated batch sizes, a 0.01 yd^3 (8 L) workabilimeter was constructed and vibrated in a manner similar to that used by Massicotte et al. (2000). This process of using the workabilimeter is outlined in Fig. 8.
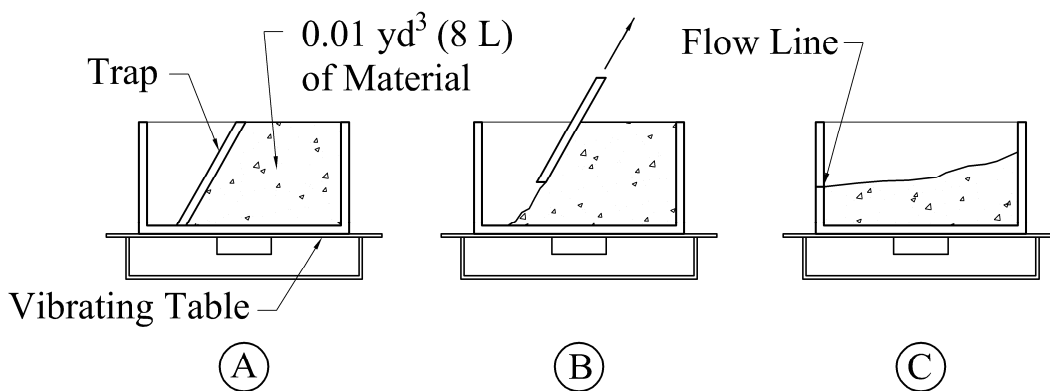
Fig. 8 – Proposed consistency measuring method

In step A, a trap is placed in the box, which is then filled with fiber reinforced material. After filling, the top is struck off level with the top of the box. In step B, the trap is removed and the stiff consistency of the fiber reinforced material maintains its form. In step C, the box is externally vibrated by a vibrating table and the time is measured for the

17

material to flow across the box and up to a pre-determined flow line. The process is repeated for different sand-to-gravel weight ratios (S/G) and the optimum mix is chosen from the mix that produces the minimum flow time. This process was carried out for the hybrid fiber gradation under consideration and the data is provided in Fig. 9. The optimum S/G was determined from a best-fit parabolic regression. A practical difference between the mix consistencies was not discernable in the range of 1.0 – 1.3. A S/G = 1.1 was chosen as an acceptable intermediate value that weighted more heavily toward the coarse aggregate side to promote a stiffer, more abrasion resistant material.
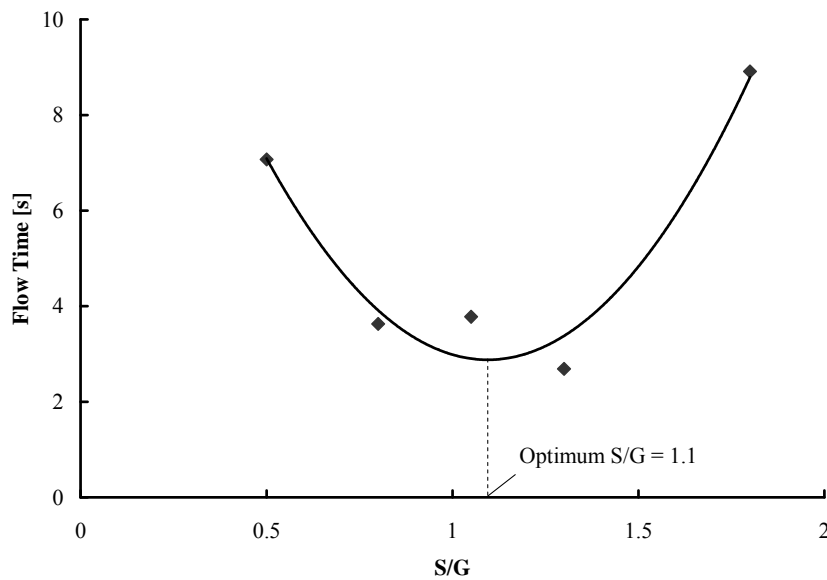
Fig. 9 – Consistency variation with sand to gravel weight ratio (S/G)

3 FLEXURAL PERFORMANCE OF ½ SCALE BRIDGE APPROACH SLABS

The existing CalTrans bridge approach slab design was used as the basis for element sizing and reinforcement ratios (Fig. 10). A longitudinal section (parallel to the flow of traffic) of the existing slab design is show in Fig.11a. It is anticipated that surface cracking in the bridge approach slab can accelerate durability related problems such as corrosion and spalling. Mechanisms for such cracking include restrained contraction due to drying and thermal mechanisms where sufficient tensile stresses develop that cause cracking. In order to approximate this behavior, ½ scale beam specimens were prepared (Fig. 11b).
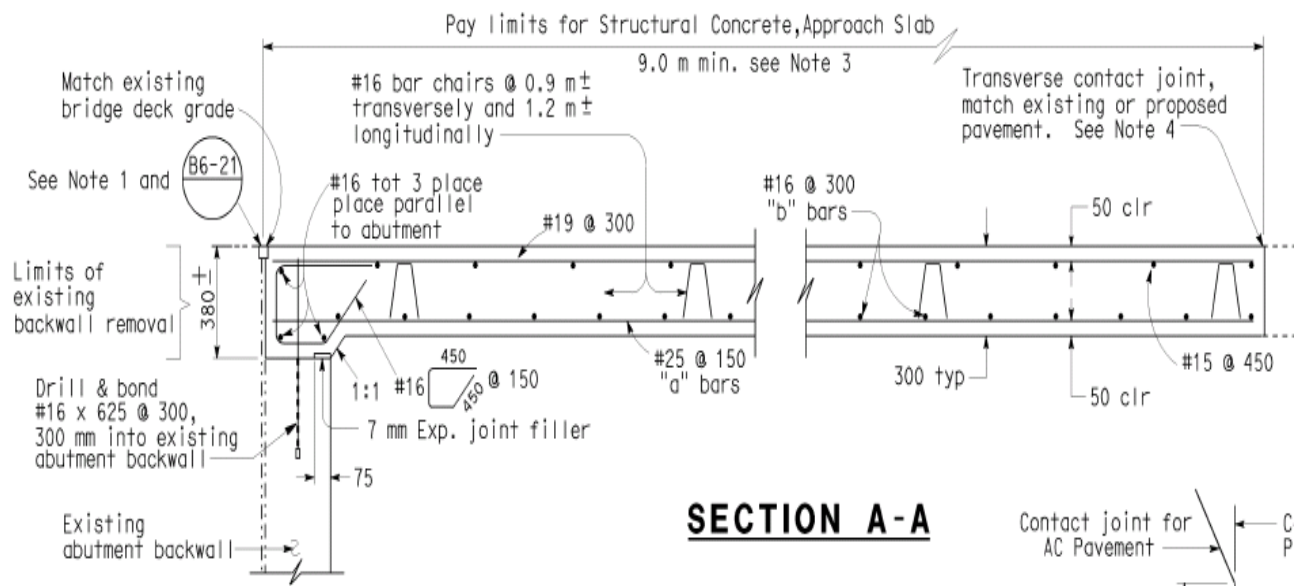
Fig. 10. CalTrans existing Bridge Approach slab design.
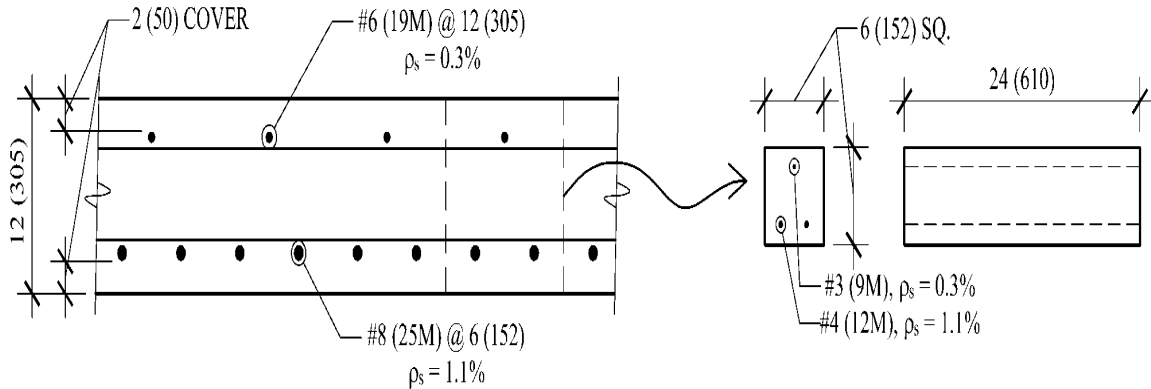
Fig .11. a) Longitudinal Section of Existing Bridge Approach Slab (BAS); b) ½ scale model of BAS

Beam specimens maintained the same dimensions shown in Fig. 6 and rebar was included in the manner shown in Fig. 12. Monotonic load-displacement tests were carried out for both un-reinforced and reinforced specimens consisting of plain concrete and the HyFRC in order to provide information regarding relative contributions of the constitutive materials to the element performance. Four conditions were tested; plain concrete, reinforced plain concrete, plain HyFRC and reinforced HyFRC. In terms of description and labeling for the remainder of this study, the use of "plain concrete" or "HyFRC" as a descriptor refers to the matrix composition only. Incorporation of the term "reinforced" refers to the use of rebar. Therefore a reinforced plain concrete specimen is an element composed of the plain concrete matrix and contains rebar.

$\#3(10M), \rho_s=0.3\%$

$1(25.4)$

$\#4(12M), \rho_s=1.1\%$

a)

b)   c)
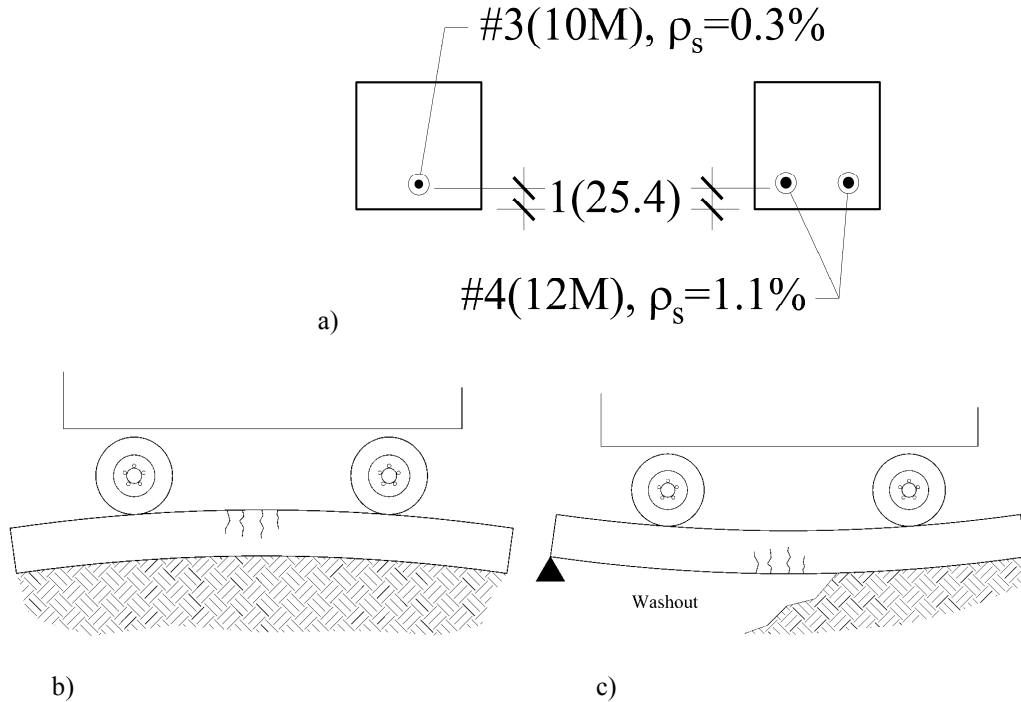
Fig. 12 – a) Rebar layout for reinforced beam element tests; b) rebar ratio of 0.3% in the tensile surface of the flexure specimens represents the top surface of the BAS and cracking associated with truck loading, drying shrinkage etc. prior to soil wash-out; c) rebar ratio of 1.1% in the tensile surface of the flexure specimens represents the bottom surface of the BAS and the cracking associated with soil wash-out.

A larger amount of HyFRC specimens were cast and tested because scatter in flexural performance due to random alignment and distribution of the fibers was anticipated. Higher degrees of repeatability were desired to justify claims about material performance. Flexure results for the plain and the lightly reinforced element series ($\rho_s = 0.3\%$) are provided in Fig. 13.   Engineering design parameters (EDP's) were defined in order to compare the relative material performance. Critical load P_c and displacement Δ_c points based on service level demands were chosen for comparison. For the plain concrete specimens this point was chosen to be the modulus of rupture. The critical points for the plain HyFRC specimens represent the maximum load (P_{max}) and the deflection at P_{max} (Δ_P).   The conventionally reinforced elements were characterized by the point of

21

conventional bar steel yield. A summary of the average EDP's for the results shown in Fig. 13 are provided in Table 4.
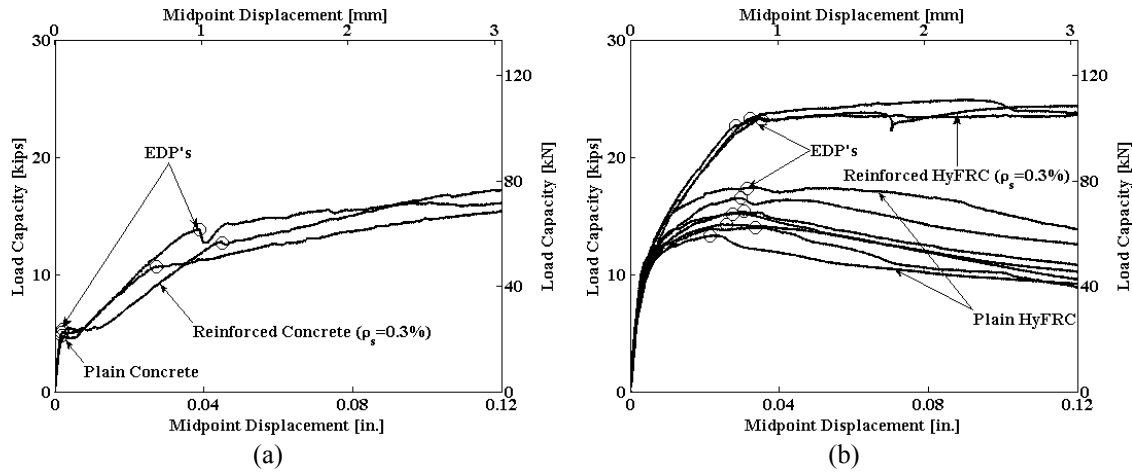
Fig. 13 – Flexure test results for (a) plain concrete and (b) HyFRC specimens

Table 4 – Experimental Flexure Test Average EDP Summary

EDP	Unreinforced		Reinforced (ρ_s=0.3%)	
	Concrete	HyFRC	Concrete	HyFRC
P_c [kips (kN)]	5.1 (22.5)	15.1 (67.3)	12.4 (55.1)	23. 0 (102.5)
Δ_c [10^{-2} in. (mm)]	0.19 (0.048)	2.85 (0.726)	3.69 (0.938)	3.20 (0.812)

Use of fiber hybridization resulted in a 196% increase in the maximum flexural strength relative to the plain concrete. Also, the corresponding flexural ductility at this point increased by an order of magnitude. Comparison of the reinforced elements ($\rho_s = 0.3\%$) shows an 85% increase in flexural strength with HyFRC. It is postulated that the strength increase was reduced when compared to the unreinforced condition because the presence of the rebar overshadows the impact of the fibers. This occurs because the flexural

strength provided by the rebar at higher ρ_s is significantly greater than the fibers are capable of providing by themselves.

The flexural results of the beam specimens with the higher reinforcing ratio (ρ_s=1.1%) is shown Fig. 14. The flexural yield strength and stiffness of the heavily reinforced HyFRC element was greater than its reinforced plain concrete counterpart, however the difference was reduced to a 67% increase in strength. An interesting phenomena is highlighted when the minimally reinforced HyFRC element (ρ_s=0.3%) is compared against the heavily reinforced plain concrete element (ρ_s=1.1%). It is evident that the reinforced concrete element is much stronger; however in the region immediately following concrete cracking the HyFRC shows a significantly stiffer behavior (Fig 14b). This response has implications for crack control that were utilized during the corrosion characterization portion of this study.

(a)   (b)
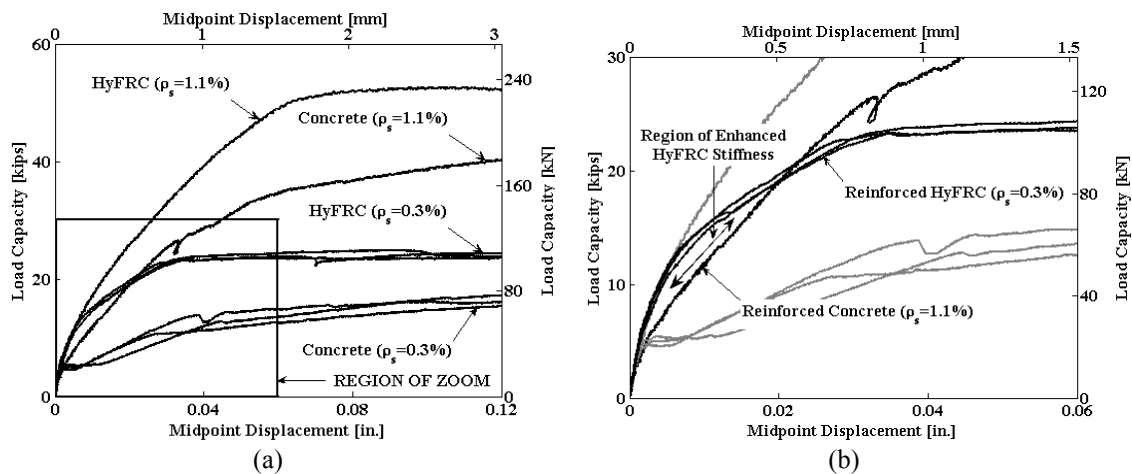
Fig. 14 – (a) Flexural performance of reinforced specimens with different reinforcing ratios ρ_s and (b) zoomed region highlighting enhanced HyFRC flexural stiffness

4   DURABILITY STUDIES

The anticipated application for the HyFRC material is as bridge approach slab located in an Area III jurisdiction.   This was chosen because demands associated with environmental conditions make reinforced plain concrete elements highly susceptible to durability related problems. This type of damage can include internalized cracking and deterioration from freeze-thaw cycling and reinforcement corrosion. Mechanisms such as these were attributed to the concrete deterioration and the subsequent shear failure that lead to the fatal collapse of the De La Concorde overpass in Quebec, Canada (Johnson et al. 2007, Wood 2008).

In the following sections, plain concrete is examined relative to HyFRC under a series of accelerated durability tests in order to determine the impacts of the proposed hybrid fiber gradation on corrosion and freeze-thaw related deterioration mechanisms. The labeling convention employed uses the "C" designation for plain concrete based specimens, while the "H" designation represents the HyFRC based specimens. Specimens may or may not contain rebar, depending on the test type.

4.1 Corrosion Initiation Experiments (Beam Specimens)

Beam specimens were used for the corrosion initiation experiments because they provided a convenient configuration to examine the impacts of flexural load induced cracking on corrosion behavior. The beams were prepared with similar dimensions to

those specified in Fig. 6 and ASTM A615 Gr. 60 rebar was added in the configuration shown in Fig. 15. The rebar configuration and specimen size were chosen to represent ½ scale strip element from a CalTrans Type R(9S) (metric designation) bridge approach slab. The matrix type varied between the CONC1 and the CONC2 (Table 2) and the beam elements were subjected to varying degrees of cyclic load based flexural demands in order to induce surface cracking. Specimens were oriented during flexural cycling such that the top surface during casting became the flexural tension surface during testing.
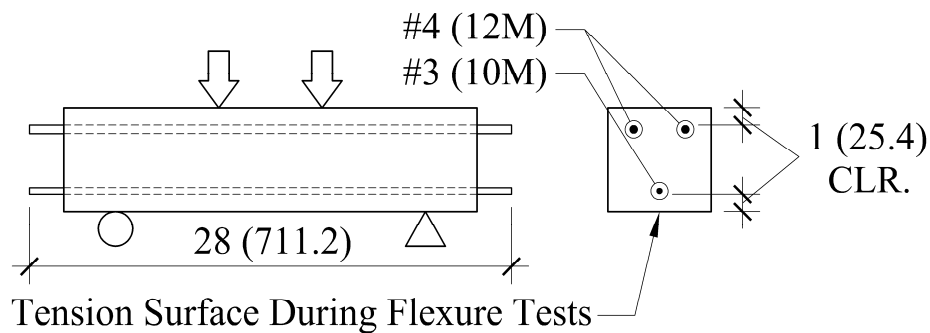
Fig. 15 – Beam specimen rebar layout and orientation during casting and testing [in. (mm)]

Corrosion of the rebar was induced by ponding a salt water solution in the configuration shown in Fig. 16 and 17. The proposed test method is very similar to that specified in ASTM G109 with the major exceptions being that the beam element dimensions have been modified and a potentiodynamic method was used for corrosion monitoring. The ponding dams were constructed out of 1/8 in. (3.2 mm) thick PVC and where adhered to the concrete surface with a Neoprene™ super flash cement caulk (brand name – EternaFlex® by Black Jack). All beam surfaces not designated as an "exposed surface" (see Fig. 16) were coated with a polymeric based sealant (brand name – Concrete Guard®

25

by Ardex). The intent behind the sealing method was to increase the driving force behind the solution's intrusion into the beam matrix. The exposed bottom surface provided the only evaporation sink, which would effectively pull the solution through the matrix and create a vertical moisture gradient.
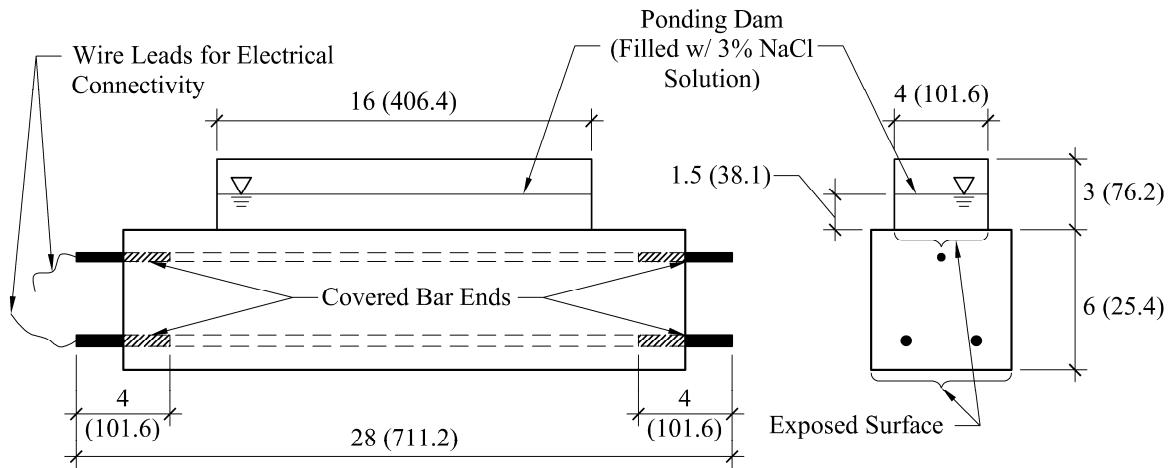
Fig. 16 – Beam specimen configuration for salt water ponding [in. (mm)]

Fig. 17 – Picture of beam specimen prepared for corrosion monitoring

The rebar surface was prepared by sandblasting in order to remove the millscale. One end of the rebar was drilled and tapped in order to provide electrical connection through a screw and ring terminal. Both ends of the rebar were painted with a layer of moisture sealant (brand name – Skotchkote[®] by 3M) and then wrapped with electrical tape and covered with a polyolefin heat shrink tube. The ends of the polyolefin tube were pinched closed and covered with the moisture sealant in order to prevent the ingress of moisture.

For corrosion monitoring, the electrochemical cell was created by placing a saturated calomel electrode (SCE) directly into the ponding dam (Fig. 18). The SCE was used as the reference electrode. The top most #3 (9M) rebar was used as the working electrode (WE) and the two #4 (12M) bottom bars were connected and used jointly as a counter electrode (CE). The beam elements were stored in a hot chamber at 122°F (50°C) at 50% RH in between corrosion monitoring periods. Evaporation of the ponded solution was mitigated by covering the ponding dams with an acrylic sheet, however it was necessary to replace the solution on a weekly basis. The old solution was completely removed by vacuuming the exposed surface and a new sodium chloride solution with the specified concentration was added.

Reference Electrode:
Saturated Calomel Electrode (SCE)

Working Electrode:
#3 (10M) ASTM 615 Gr. 60
Reinforcing Steel

Counter Electrode:
2- #4 (12M) ASTM 615 Gr. 60
Reinforcing Steel
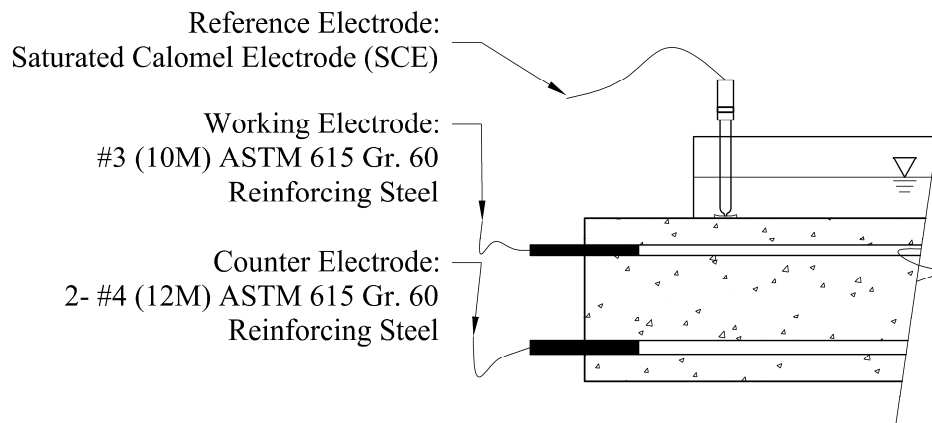
Fig. 18 – Embedded cell for corrosion monitoring experiments

Corrosion monitoring was carried out through a series a direct current (DC), potentiodynamic measurements. An EG&G Princeton Applied Research model 363 potentiostat was used for this purpose. The experimental set-up also consisted of a custom built ramp signal generator which was used to control the rate of potentiodynamic sweeps and a Measurement and Computing USB-1208LS data acquisition (DAQ) module for automated data recording. The DAQ interfaced directly via USB with a personal computer (PC), where data was stored. This monitoring setup is illustrated schematically in Fig. 19.
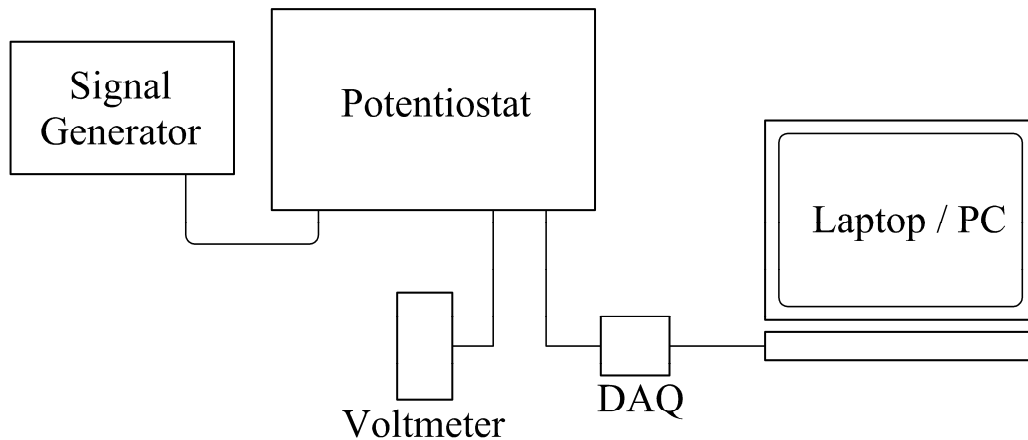
Fig. 19 – Schematic of corrosion monitoring setup

Polarization resistance (PR) measurements were performed in a similar manner to that specified in ASTM G59-97. Upon removal from the hot chamber, specimens were immediately clipped in to the potentiostat and the corrosion potential (a.k.a. open circuit potential) E_{oc} was recorded at equilibrium. Equilibrium was specified when a 0.1 mV shift in E_{oc} was not detected over a 1 minute interval (typically occurred within 5 minutes

28

of the start of monitoring). Scans were carried out in the anodic direction with a span of ± 10 mV relative to the E_{oc} at a rate of 10 mV/min. Specimens were cathodically conditioned at $E_{oc} - 10$ mV for 30 seconds prior to initiation of the PR scan. An example of the measurement results with data regression is provided in Fig. 20.
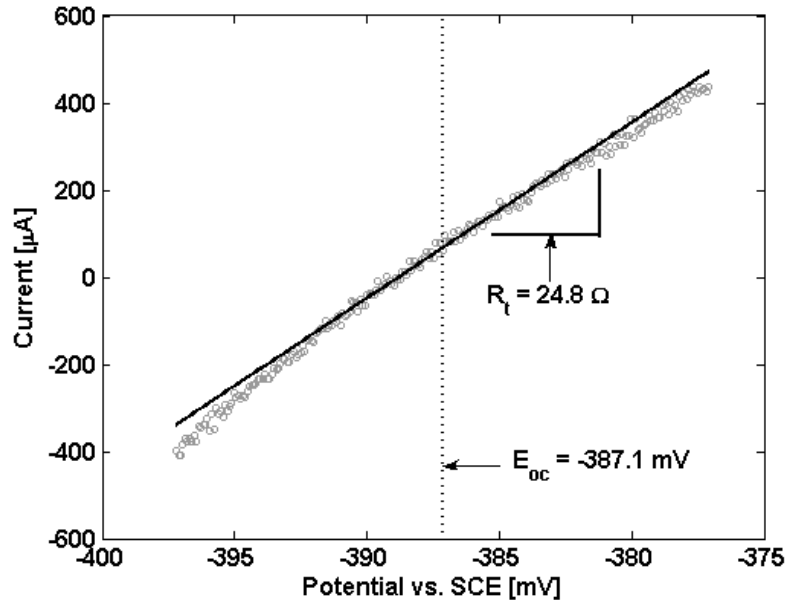
Fig. 20 – Example polarization resistance measurement

The total resistance of the cell R_t was calculated from the data by determining the tangent to experimental curve at the E_{oc}. For purposes of this experimental study the tangent was approximated by a linear regression of the data points within ± 5 mV relative to the E_{oc}. Due to the offset of the reference electrode from the WE in the beam corrosion cell (see Fig. 19) it was anticipated that a relatively large component of R_t would be the electrolytic resistance R_e inherent in the portion of the concrete based matrix that separated the two electrodes. The potentiostat had a built in analog feedback component used for IR compensation that allowed for the direct determination of R_e. This was a

29

necessary step given that the use of metallic, electrically conducting fibers in the matrix could significantly influence its value. The magnitude of the polarization resistance at the rebar surface of concern (the WE) could then be determined from

$$R_p = R_t - R_e \tag{4.1}$$

If it is assumed that an equivalent initial condition is present among the specimens, relative comparisons of the corrosion behavior can be made with knowledge of R_p alone. For instance, higher rates of corrosion would be expected in specimens with lower values of R_p when compared to other specimens with larger R_p. However, if more information is desired that can allow for the determination of the rates of rebar dissolution and corrosion product formation, R_p needs to be converted to a corrosion rate i_{corr}. Precise corrosion rate measurements are particularly difficult, especially when multiple measurements are desired over a prolonged period of time. For this reason PR is an adequate method because the system is relatively undisturbed from the small scans that are necessary to get an accurate measurement.

In order to determine the corrosion current density i_{corr} from R_p the Stearn-Geary coefficient B is necessary. It is defined as

$$B = \frac{\beta_a \beta_c}{2.303(\beta_a + \beta_c)} \tag{4.2}$$

where β_a and β_c represent the anodic and cathodic Tafel slopes respectively. The corrosion current density is then

$$i_{corr} = \frac{B}{R_p \cdot A} \tag{4.3}$$

where A is the exposed area of the WE. The Tafel slopes can be determined from large sweep polarization measurements. At potentials far from E_{oc}, the measured cell current is representative of the actual anodic or cathodic kinetics (depends on whether the polarization direction is anodic or cathodic relative to the E_{oc}). Accepted values for corrosion in reinforced concrete range from $B = 26$ mV in active corrosion to $B = 52$ mV while passivated (Andrade & Gonzalez 1978, Andrade & Alonso 1996). Due to the fact that B is assumed a priori in order to conduct repetitive, non-destructive corrosion rate determinations, it is understood that a certain amount of error is to be expected when electrochemical estimates of mass loss are compared against gravimetric. The average value of $B = 26$ mV was adopted for the determination of corrosion rates in this study with the understanding that the maximum error in the measurement is a factor of 2 (Andrade & Alonso 1996). This error would be under consideration when comparisons of the electrochemical data are made.

It was also desired to characterize the galvanic current I_g flow between the WE and CE. This was achieved by creating a galvanic couple between the WE and CE by coupling the wire leads during storage in the hot chamber. This approximates a potential corrosion mechanism in bridge decks and slabs where two layers of reinforcement are used. Chairs made of rebar are fabricated and placed in between the two layers in order to provide a spacer during fabrication. The chairs remain in the slab when the concrete is placed, providing a direct electrical connection between the top and bottom layer. The galvanic (macro) cell is created when one layer undergoes active corrosion (either from Cl⁻ or CO_2 intrusion) and the other remains passive. This current was measured with the EG&G model 363 potentiostat by using it as a zero resistance ammeter (ZRA). Specimens were

removed from the hot storage chamber and immediately coupled in to the ZRA. The current was sampled at a rate of 2 Hz for 2 minutes. It was noted that a relatively steady state current flow I_{ss} was attained within 30-40 seconds of monitoring, so the galvanic current was determined by averaging over the data taken from 60 to 120 seconds within in the monitoring interval. This is shown in Fig. 21.
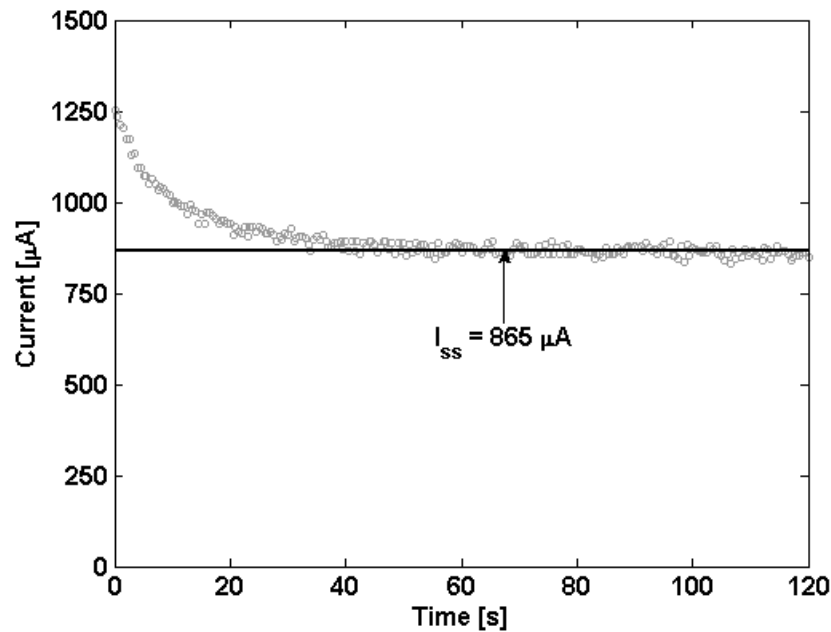
Fig. 21 – Example macrocell (galvanic current) measurement

The following reports and discusses the results of the beam corrosion monitoring series. The beams were prepared and tested in 3 conditions; (1) uncracked, (2) cracked under similar flexural displacement demands and (3) cracked under similar load based demands. The convention for reporting the electrochemical data is as follows; the individual data points are provided and a continuous average curve is shown for each matrix type that represents an idealized continuity between the corrosion monitoring

intervals. This method was deemed acceptable because solution cycling was not employed so that the behavior, as measured, is an equilibrium behavior that can be assumed to persist in between the monitoring intervals.

4.1.1 Uncracked Beam Specimens

The first series of beam specimens were prepared with a CONC1 matrix and cast and cured (7 day wet, 21 day dry) as described previously. At the conclusion of the curing period, ponding dams and were immediately adhered to the top surface during casting and the outer surfaces were coated with sealant. Ponding started 1 week following application of the sealant. The corrosion potential E_{oc} and the estimated corrosion current density i_{corr} based on the polarization resistance R_p measurements were measured periodically through an 80 week monitoring period. These results are provided in Figs. 22 and 23.
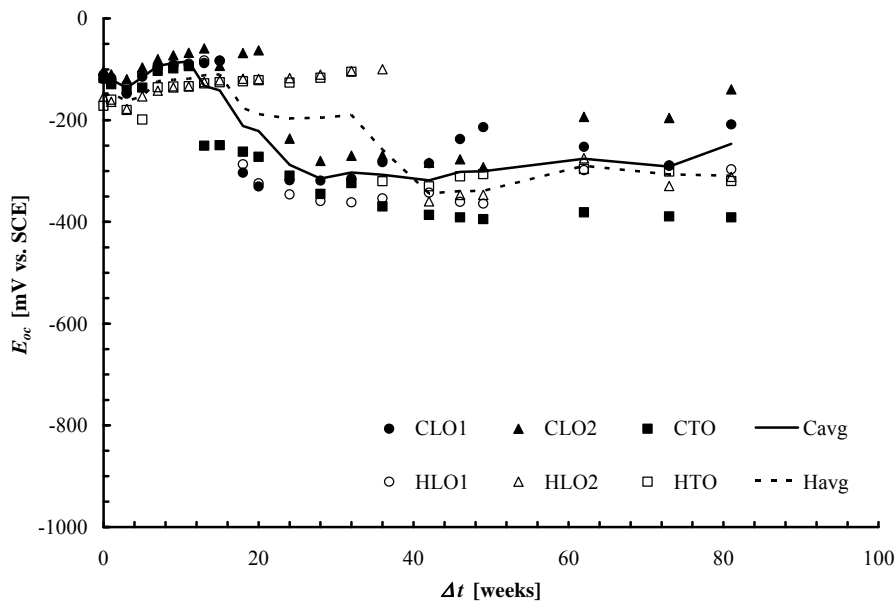
Fig. 22 – Uncracked beam specimen corrosion potentials
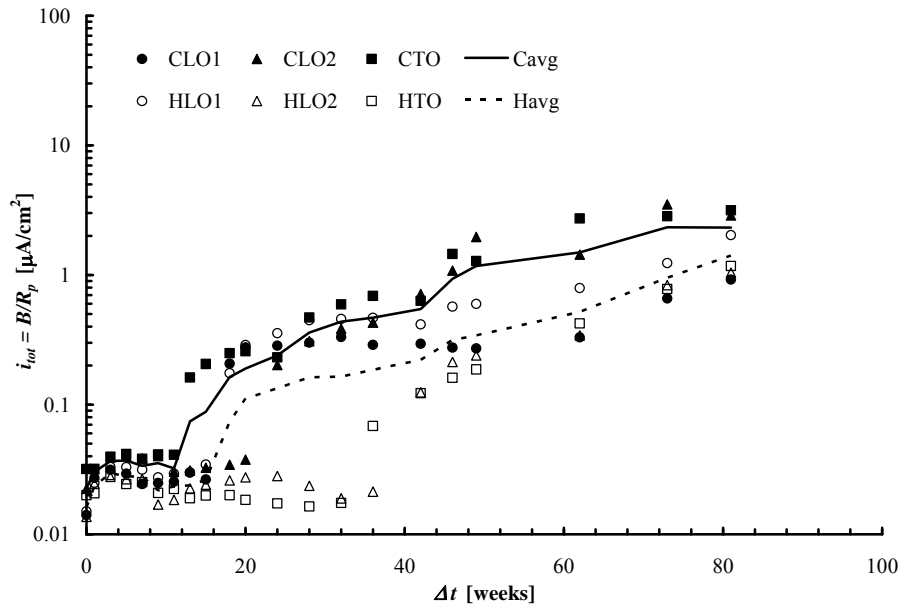
Fig. 23 – Estimated uncracked beam specimen corrosion current densities

The two monitoring techniques are consistent in that more positive E_{oc} values corresponded to lower values of i_{corr}. Initially, all specimens showed corrosion rates reflective of a passive behavior of the rebar. It wasn't until 12 weeks after the start of ponding that the first of the specimens (CTO) showed corrosion initiation with $i_{corr} \sim 0.2$ $\mu A/cm^2$. Within 24 weeks all the plain concrete "C" type specimens showed active corrosion rates while it took nearly 44 weeks for all the HyFRC "H" type specimens to reach active corrosion rates. The delay in active corrosion for the HyFRC specimens can be attributed to the relatively aggressive curing regime, where dry curing was used for the bulk of the 28 day interval. Moisture evaporation at the surface of the specimen induced localized drying shrinkage which produced cracking that compromised the effectiveness of the concrete cover. The presence of the fibers in the HyFRC provided increased crack resistance at the surface, delayed the ingress rates of Cl⁻. This observation is consistent

34

with other experiments concerning fiber reinforced materials and corrosion (Al-Tayibb 1990).

Once active corrosion was observed in all specimens, however, the difference between the average corrosion rate in the plain concrete and the HyFRC was relatively small (varies between a factor of 2-3). This observation, coupled with the anticipated error in the proposed monitoring method (factor of 2) makes conclusions regarding a difference in corrosion propagation rates unclear. This behavior will be discussed in more detail within the context of the corrosion propagation specimen of section 4.2.

4.1.2 Cracked Corrosion Beam Specimens (Displacement Demand)

Three beam specimens for both the plain concrete and the HyFRC were prepared with a CONC1 matrix in an identical manner to those described in section 4.1.1. Following the 28 day curing period, the specimens were cycled in flexure using the testing configuration specified in Fig. 15. This induced tensile stresses at the surface containing the WE, which would subsequently be monitored for corrosion. Based on the results from previous testing (see Fig. 13), load based demands were chosen such that both the plain concrete and HyFRC specimens would development similar displacement demands in the cracked regime (load demands exceed the plain concrete modulus of rupture) and the rebar would not yield. Five complete cycles of load and unload were performed in order to initiate and propagate the surface cracking. The results of the cyclic mechanical tests are provided in Fig. 24 followed by a schematic representing the position of the cracks on the beam tensile surface (Fig. 25). High resolution (2400 dpi) surface scans are

also provided in Figs. 26 and 27 in order for a more accurate visualization of the surface

cracking behavior.
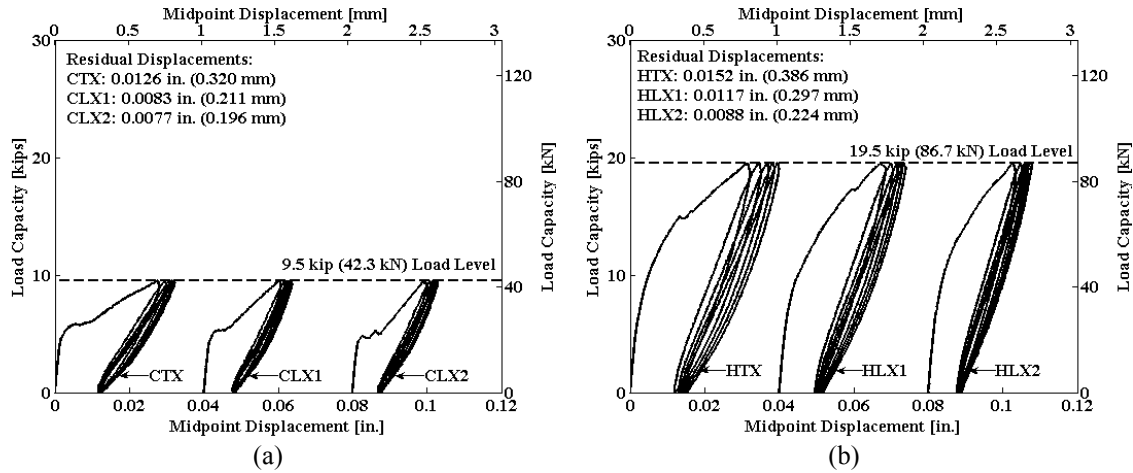
Fig. 24 – Cyclic flexure behavior for (a) reinforced plain concrete and (b) reinforced HyFRC
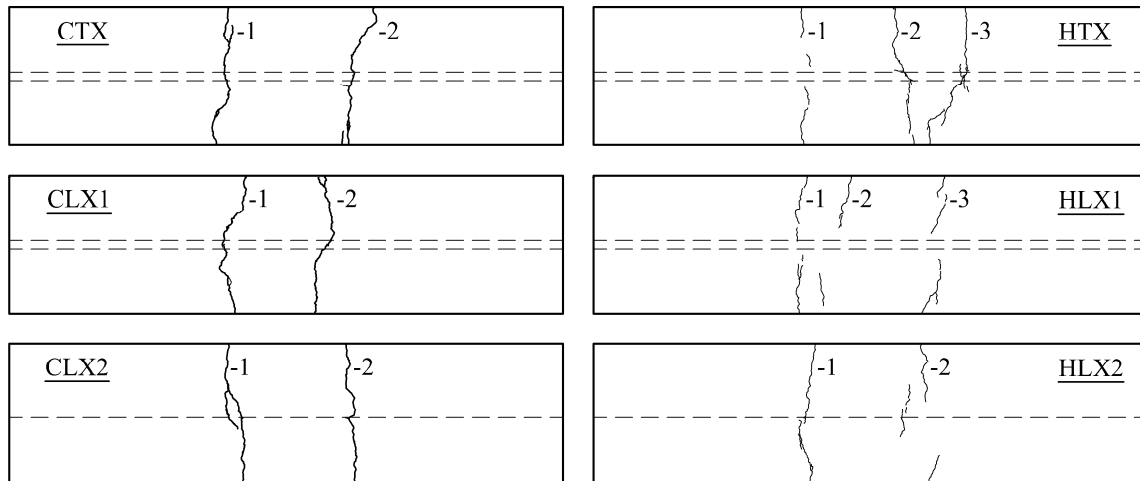
Fig. 25 – Cracked beam (similar displacement demand) tensile surfaces after cyclic flexure tests (dashed line represents position of the tensile rebar)

36
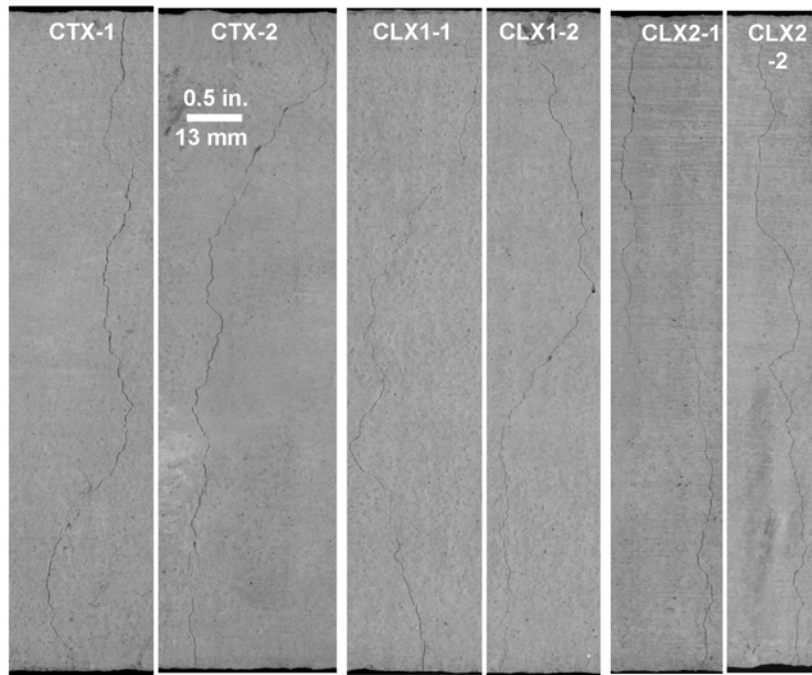
Fig. 26 – High resolution digital surface scans of reinforced plain concrete surfaces after cyclic flexure tests
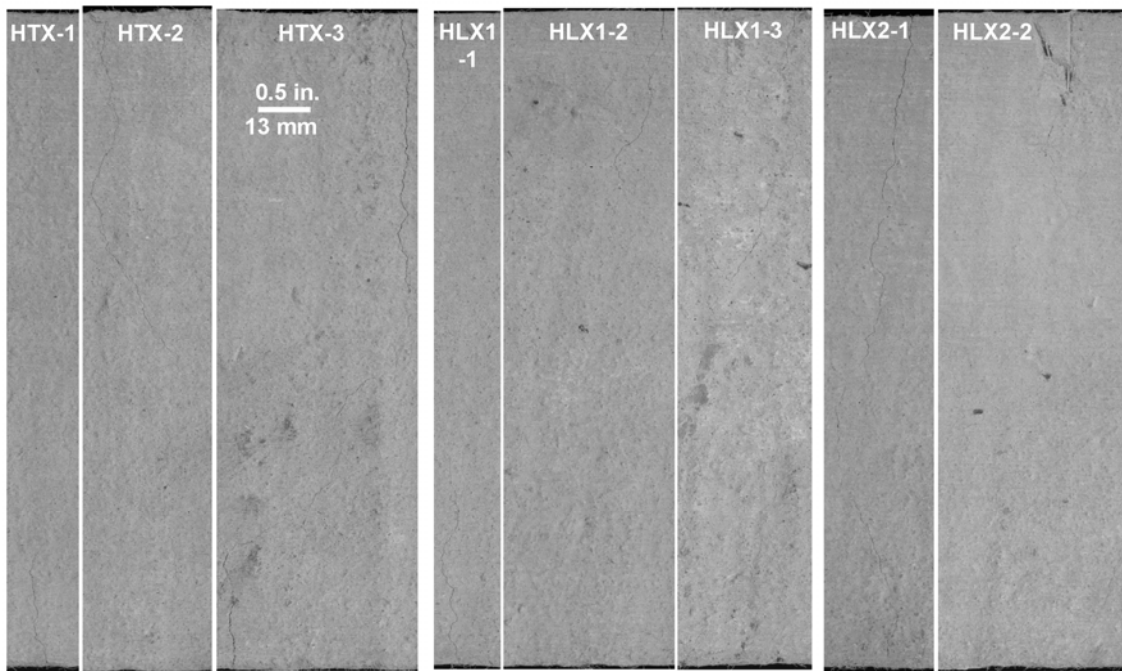
Fig. 27 –High resolution digital surface scans of the reinforced HyFRC surfaces after cyclic flexure tests

A comparison between the cyclic flexural performance shows that more than 2x the load demand was necessary to produce similar displacements in the reinforced HyFRC specimens when compared to the reinforced plain concrete at a load level just below the rebar yield point. This reaffirms the observation that significant increases in the monotonic flexural stiffness occur in the presence of the HyFRC mix (see also Fig. 14). However, once the specified load demands were reached for each specimen, a comparison between the cracked stiffness shows they were nearly identical.

A comparison of the cracked surfaces following the cyclic testing (Fig. 25) showed that two well defined transverse (perpendicular to the direction of the rebar) cracks appeared in the reinforced plain concrete specimens, while the HyFRC specimens produced 2 and 3 distinct cracks. The nature of the surface cracking in the HyFRC was more difficult to characterize because the cracks were smaller in width and not continuous over the surface of the beam meaning they typically disappeared from view (within the 4×10^{-4} (10 μm) pixel resolution of the scanning method) over the top of the rebar. The fine cracks in the HyFRC specimens shown in the digital scans provided in Fig. 27 can be most easily viewed in the original word document of this report when the viewer uses a zoom of 500%.

Following cyclic testing, the ponding dams were adhered to the cracked surface of the beam and the sides were coated with sealant. Salt water ponding began 1 week following the application of the sealant and corrosion monitoring commenced. The data for the corrosion potential E_{oc} and the estimated corrosion current density i_{corr} are provided in Figs. 28 and 29.

Fig. 28 – Cracked beam (similar displacement demand) specimen corrosion potentials
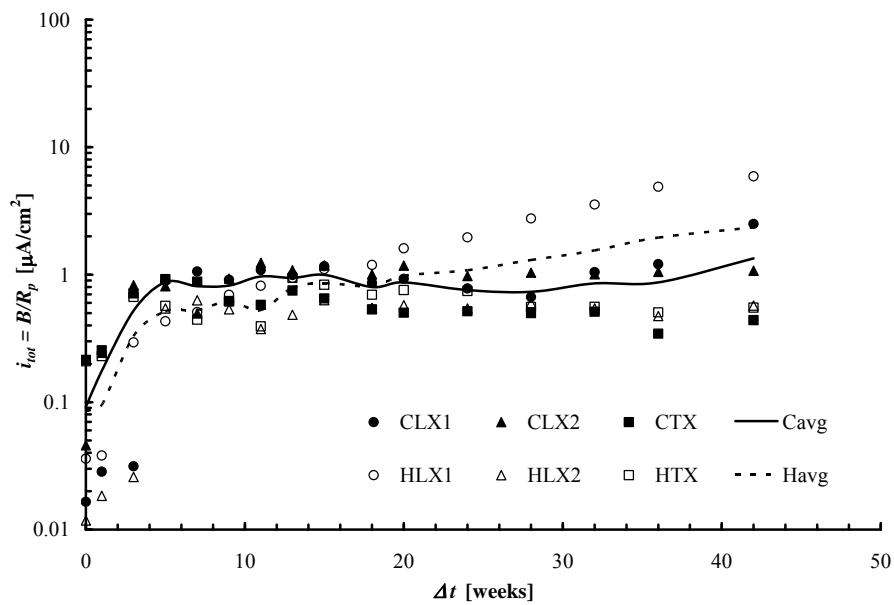
Fig. 29 – Estimated cracked beam (similar displacement demands) specimen corrosion current densities

The monitoring method was consistent in the manner described in section 4.1.1; more positive values of E_{oc} corresponded to lower values of i_{corr}. However, in contrast to the uncracked beam specimens reported on previously, all specimens reached active corrosion rates within 4 weeks after the start of ponding and no noticeable difference was apparent between the reinforced plain concrete and the reinforced HyFRC. Corrosion monitoring was concluded after 42 weeks of ponding, when corrosion rates equivalent to the uncracked specimens after 80 weeks of ponding, was observed. Also, similar to the uncracked specimens, a distinction between the material types was difficult when the relative difference between the average corrosion current densities varied between a factor of 1 to 2.

4.1.3 Cracked Corrosion Beam Specimens (Load Demand)

Another beam series was prepared for equivalent load based cyclic flexural demands. A CONC2 matrix was used for this beam series and the specimens were prepared, cast and cured in the same manner described previously (sections 4.1.1 and 4.1.2). Four point cyclic bend tests were carried out in the manner shown in Fig. 15 and these results are provided in Fig. 30. Schematics and high resolution scans of the tensile surface cracking follow in Figs. 31 and 32.
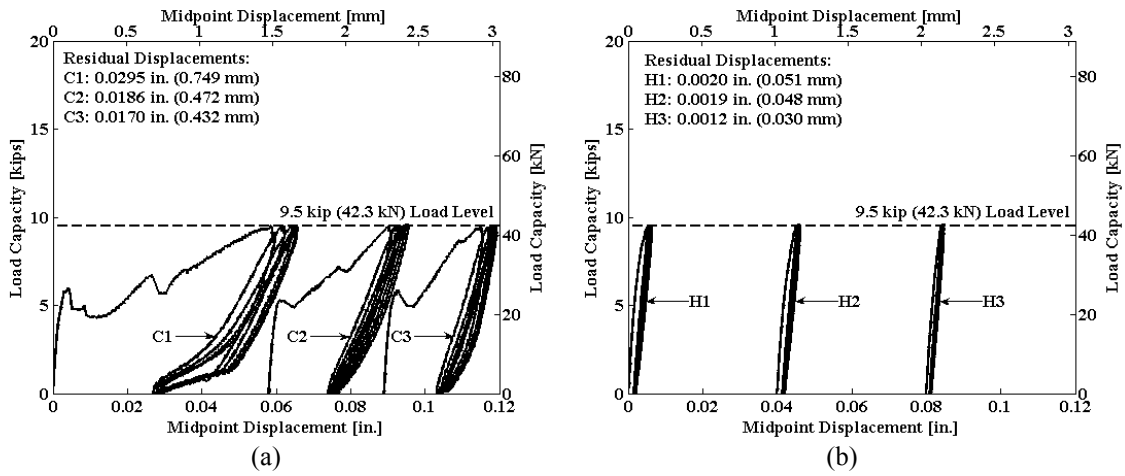
Fig. 30 – Cyclic flexure behavior for (a) reinforced plain concrete and (b) reinforced HyFRC
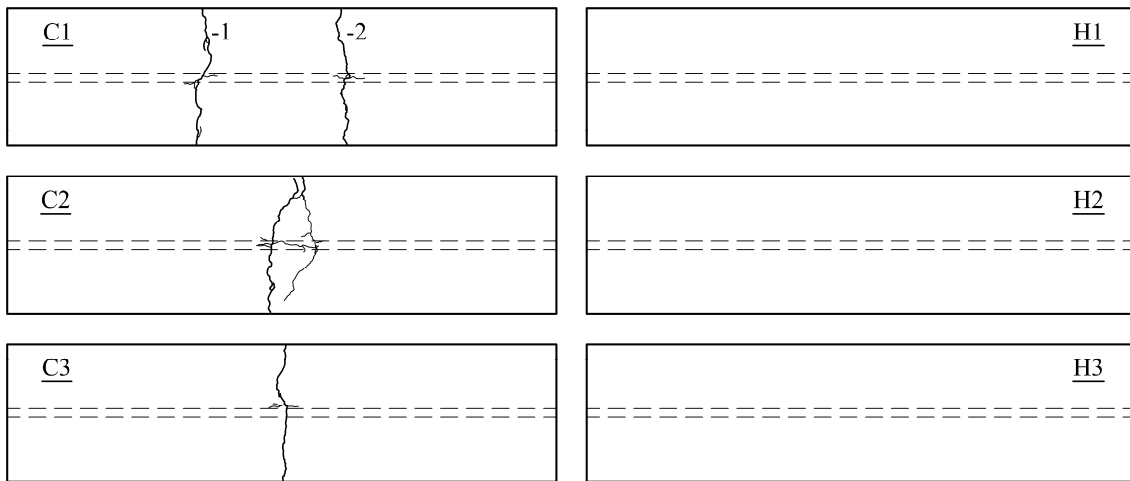
Fig. 31 – Beam tensile surfaces after cyclic flexure tests (dashed line represents position of the tensile rebar)
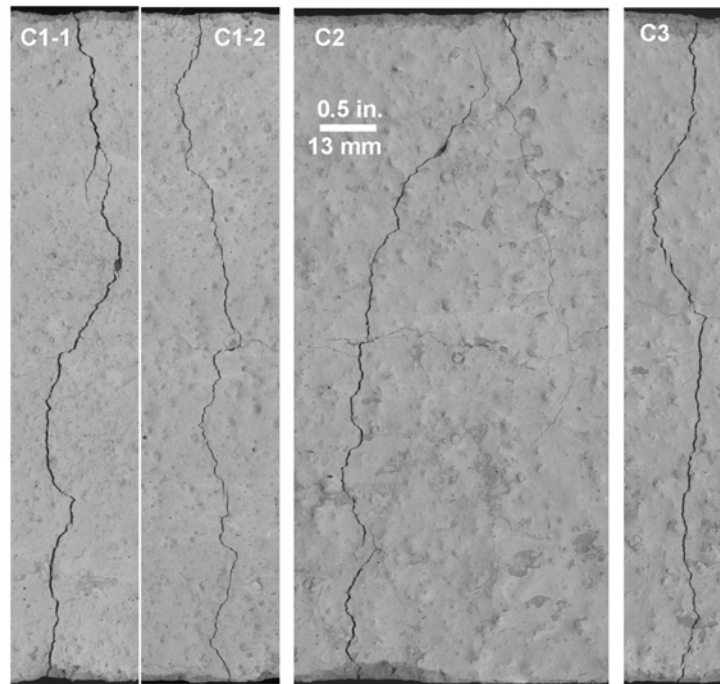
Fig. 32 – High resolution digital surface scans of the reinforced plain concrete after cyclic load testing

The mechanical data for the reinforced plain concrete specimens is similar to that shown in Fig. 30(a) with matrix cracking occurring near 5 kips (22.2 kN) of load followed by a region of reduced flexural stiffness. The reinforced HyFRC specimens, under an identical load based demand, show a significantly higher flexural stiffness loads greater than 5 kips (22.2 kN) and in the cyclic regime. Note that in Fig. 32 surface cracks are not shown on the reinforced HyFRC specimens because none were detectable through direct visual examination.

Following cyclic testing ponding dams were adhered to the surface and the sealant was applied to the sides. Salt water ponding was started 1 week following application of the dams and sealant. The values for the corrosion potential E_{oc} and the total corrosion current density i_{tot} are provided in Figs. 33 and 34. During storage in the hot chamber,

the bottom bars (CE) were electrically connected to the top (WE) so a macrocell was formed. The macrocell (galvanic) current density i_g is provided in Fig. 35.
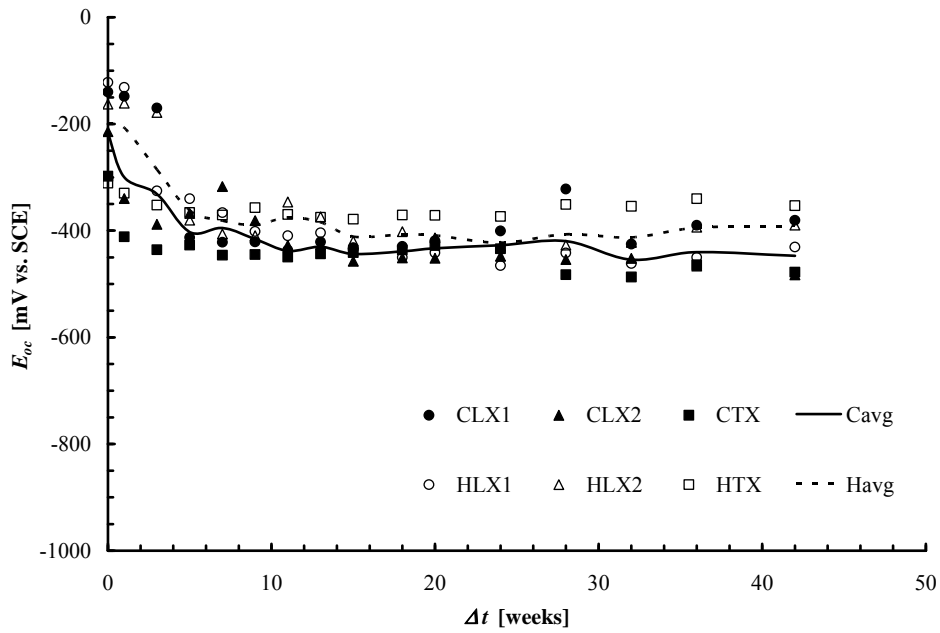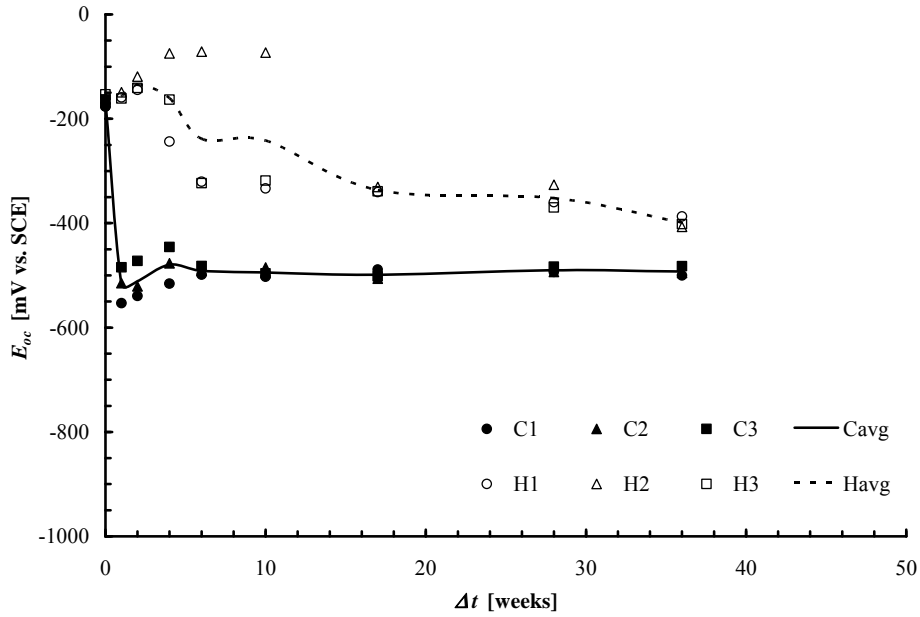

Fig. 33 – Cracked beam (similar load demand) specimen corrosion potentials
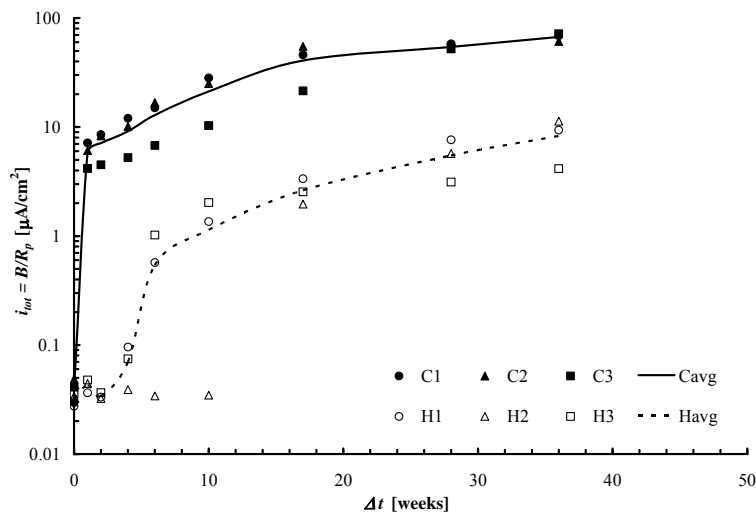
Fig. 34 – Estimated cracked beam (similar load demands) specimen corrosion current densities

43
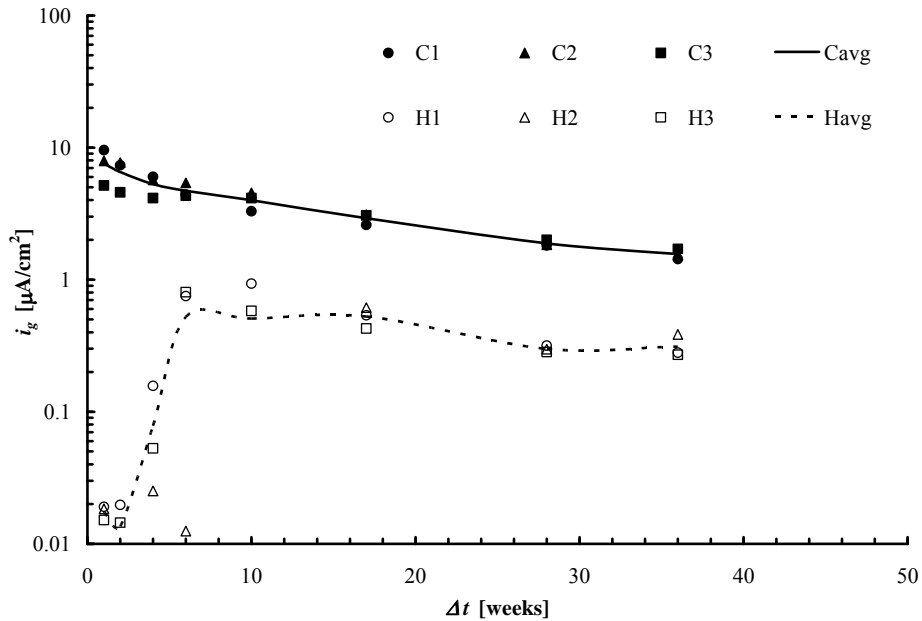
Fig. 35 – Cracked beam (similar load demands) specimen macrocell corrosion current densities

The electrochemical data shows a significant difference between the specimen types, with the reinforced HyFRC specimens having lower corrosion rates (both i_{tot} and i_g). The average difference ranges between a factor of 8-10 along the corrosion monitoring interval, which is well outside the range of the anticipated 2x error. Corrosion in the reinforced plain concrete specimens was significant enough such that corrosion products were visible at the crack surface. This is shown in Fig. 36.
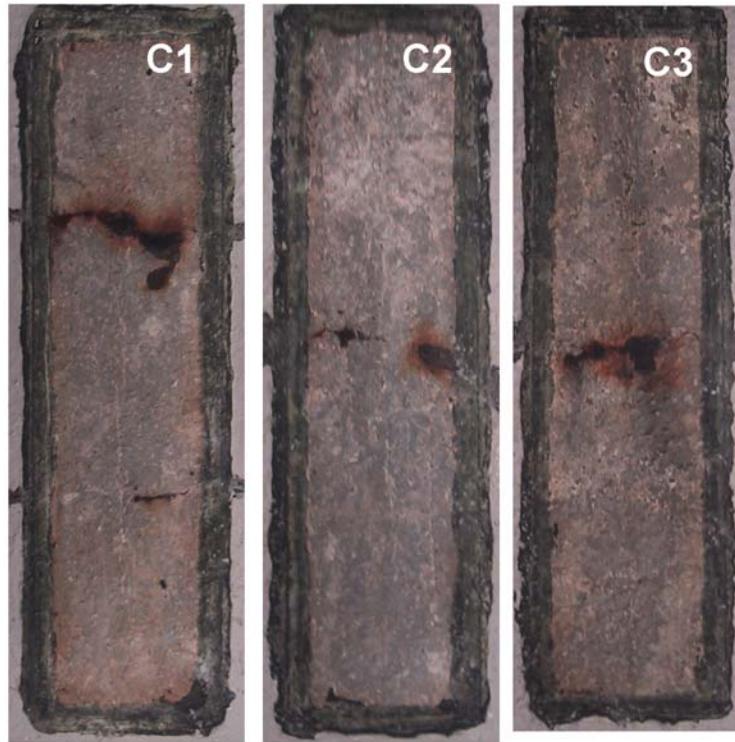
Fig. 36 – Reinforced plain concrete surface condition following salt water ponding (the black rectangular shape at the periphery of each specimen is the residue from the mastic caulk used to adhere the ponding dams to the concrete surface)

In order to provide a more rigorous method for comparison, the discrete data points for both i_g and i_{tot} can be numerically integrated to give a value of the total corrosion charge transfer Q_{tot}. A numerical integration scheme was employed in the following manner

$$Q_{tot} = A \sum_{k=1}^{n-1} \frac{1}{2} \left(\Delta t_{k+1} - \Delta t_k \right) \left(i_{k+1} + i_k \right) \tag{4.4}$$

where A is the area of the exposed WE, Δt is the time interval when the corrosion measurement was conducted, i is corrosion current density (could be either i_g or i_{tot}) and n is the total number of corrosion measurements taken per specimen. This calculation was carried out for all specimens and is summarized in Table 5.

Table 5 – Total charge transfer Q_{tot} estimates for both i_g and i_{tot} measurements [units = C]

Specimen	Galvanic Q_g	Total Q_{tot}
C1	1.01×10^4	1.36×10^5
C2	1.14×10^4	1.34×10^5
C3	1.01×10^4	0.99×10^5
H1	1.54×10^3	1.38×10^4
H2	0.92×10^3	1.08×10^4
H3	1.23×10^3	0.77×10^4

A comparison amongst the values of Q_{tot} for the different specimen types shows that in both cases (galvanic and total) the corrosion charge transfer differs by an order of magnitude, with the plain concrete samples having the larger values. It is also interesting to note that a comparison between the different methods of corrosion rate determination (i_g and i_{tot}) result in charge transfers that also differ by an order of magnitude. This highlights the importance of method choice when determining the actual corrosion rates at the rebar of concern.

The significant difference in the specimen behavior warranted further study. A series of destructive tests were conducted to characterize the material post corrosion behavior. Monotonic, 4 point flexure tests were performed on 2 of the 3 samples for each material type and these results are presented in Fig. 37.
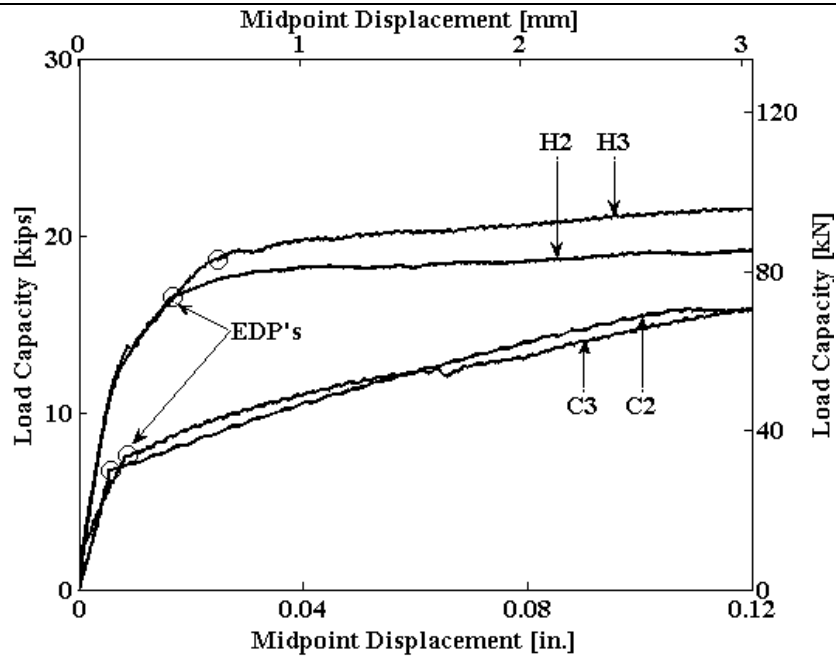
Fig. 37 – Monotonic flexure tests following 9 months of salt solution ponding

Note that cyclic flexural tests up to a load level of 9.5 kips (42.3 kN) were conducted on these specimens prior to salt solution ponding and that the load level was chosen so as to maximize the reinforced plain concrete cracked displacement while not exceeding the yield strength of the rebar. In Fig. 37 the yield point of the rebar is highlighted as the EDP for both the reinforced plain concrete and reinforced HyFRC specimens. For both of the reinforced plain concrete specimens, the yield point of the rebar fell below the 9.5 kip (42.3 kN) mark, suggesting that significant section loss from corrosion had occurred where the rebar bridged the crack. In specimen C2, the post-yield flexural stiffness began to flatten near a displacement demand of 0.12 in. (3 mm) so flexural testing was continued until rebar fracture occurred at an ultimate displacement of 0.1225 in. (3.1 mm).

Following the flexure tests, the beam specimens underwent a series of procedures designed to determine the Cl⁻ concentration through the depth of the specimen and to

extract the corroded rebar for visual and gravimetric assessment. In order to conduct the

Cl⁻ concentration measurements 1.25ϕ x 3 in. (31.8ϕ x 76.2 mm) cores were taken

through the top surface of beam element adjacent to the WE. One core was taken from

the central region of the beam, however for the case where visible surface cracks were

present during corrosion monitoring (plain concrete specimens) two cores were taken;

one adjacent to the crack and another relatively far {3-4in. (76.2-101.6mm)} from the

crack (Fig. 38). Core samples were dry cut in to 1 in. (25.4 mm) long segments to

characterize the Cl⁻ concentration with depth. They were then prepared and tested per

ASTM C1152 for acid soluble chloride content. These results are provided in Fig. 39.
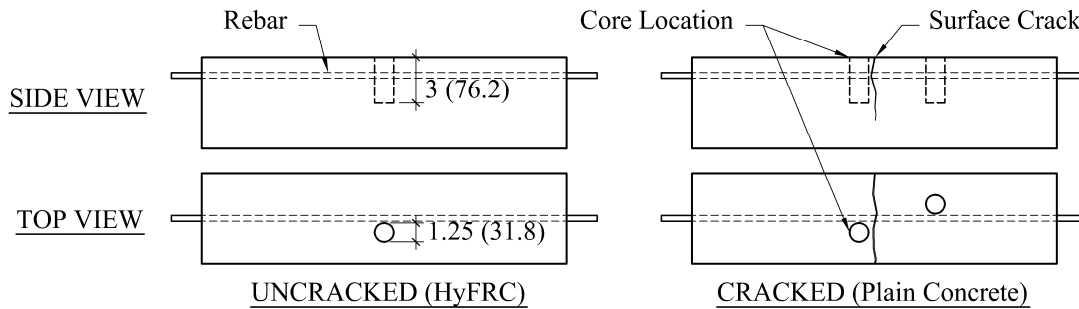
Fig. 38 – Schematic of core extraction location in beam specimens [in. (mm)]
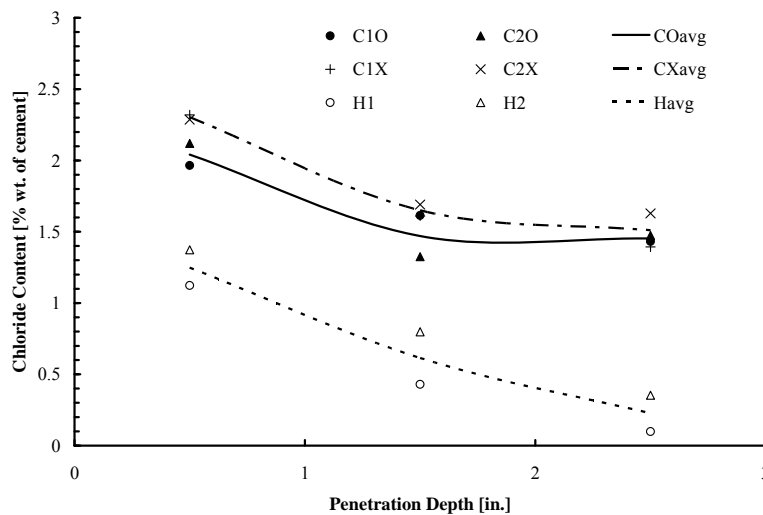
Fig. 39 – Chloride concentration profiles

Examination of Fig. 39 shows a clear distinction between the HyFRC and plain concrete specimens, which is consistent with the electrochemical data. However, the distinction between the CO and CX specimens is not as clear. Some sensitivity to the transverse crack is apparent with slightly higher Cl⁻ concentrations in the CX specimens, however the difference between the "C" type and "H" type is much greater. It was anticipated prior to testing that the CO specimens would show Cl⁻ concentrations very similar to the H type because the cores were taken sufficiently far from the crack to represent an uncompromised matrix. Surface examinations of the "C" type beams after cyclic loading, prior to the start of ponding, provided validation for this assumption because surface cracks were not visible. However, the data suggests some mechanism is present in the "C" type specimens that is effectively increasing their permeability to Cl⁻.

One possible explanation could be the presence of internal cracking from bond stresses. The magnitude of cracking is dependent on multiple factors which include the load on the rebar, the geometry of the rebar and the quality of and thickness of the surrounding concrete. Figure 40 schematically represents possible modes of cracking from rebar/matrix bond interaction which was shown to exist by others (Tepfers 1979). A close examination of the high resolution digital scans in Fig. 32 shows that fine cracks are present which are parallel to the rebar. This is consistent with splitting bond failure. Due to the fact that the cores were extracted adjacent to the rebar, any internalized system of cracking that propagates from the surface of the rebar would increase the effective permeability of surrounding portions of the matrix which would show up in the Cl⁻ concentration profiles. The presence of the fibers in the H type specimens would assist in

resisting this mechanism of cracking by two means. First, due to the fact that load based demands were used in flexure, the presence of the fibers effectively reduces the load demand on the rebar, thereby reducing the bond stresses that develop between the bar and matrix. This alone may have been sufficient to prevent cracking. Secondly, if cracks had formed the fibers would provide sources of toughening in the matrix, thereby reducing the magnitude of crack propagation and growth. It is important to note that the relatively aggressive curing regime of the beams (7 day wet, 21 day dry) may have contributed to cover cracking through mechanisms such as drying shrinkage. These explanations could not be verified directly, however, because of the destructive nature of core sampling and bar removal. Experiments utilizing epoxy impregnation should be performed on similar specimens to verify the validity of this mechanism.
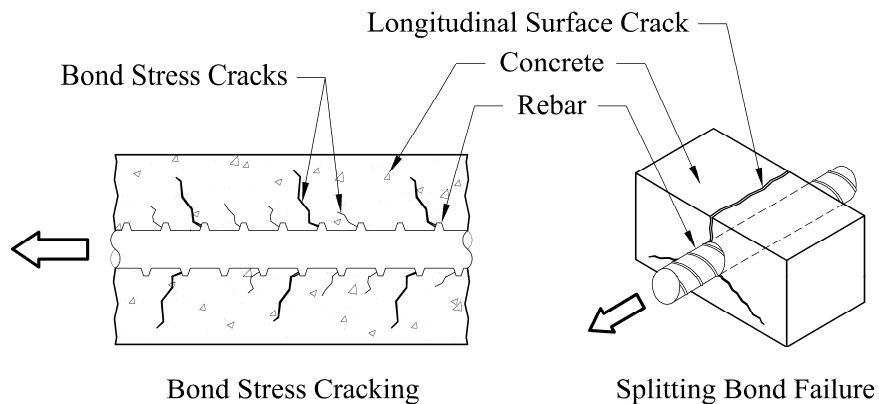
Fig. 40 – Cracking mechanisms from rebar/matrix bond interaction

Following core extraction, the rebar was removed by destroying the surrounding matrix. The amount of corrosion product deposition along the bar was noted (see Figs. 41 and 42) and the rebar were then cleaned in an acid bath per ASTM G1-03. Following cleaning, the bars were immediately weighed and digital scans were made of the area of greatest

50

section loss (see Fig. 43). Note that the pictures and scans (Figs. 41 – 43) can be adequately examined in detail in the original digital word document under a magnification of 500%.
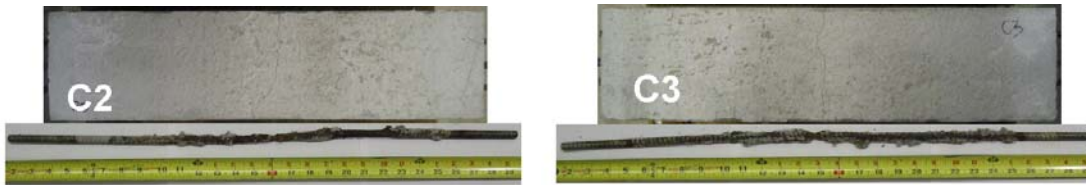
Fig. 41 – Corroded rebar in plain concrete beam specimens
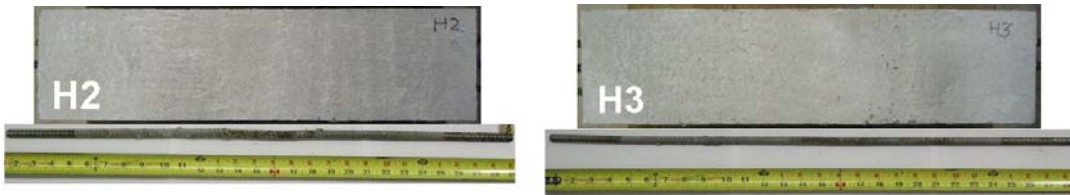
Fig. 42 – Corroded rebar in HyFRC beam specimens
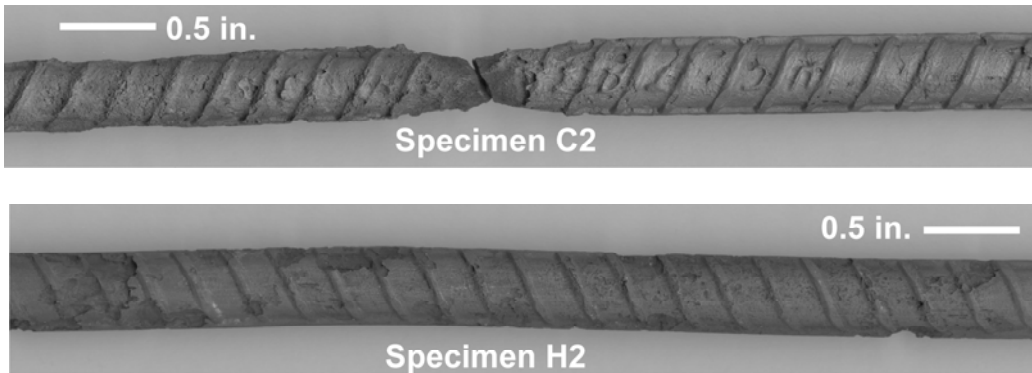
Fig. 43 – High resolution digital scans of the region of greatest section loss

It is noted that the 4 in. (101.6 mm) end segments of all the bars were tapped and covered to prevent exposure during corrosion testing which is the reason for the discoloration in the figures. Corrosion product deposition was observed over 87% and 99% of the exposed top surface area of the bars in specimens C2 and C3 respectively with a region of

localized section reduction at or adjacent to the location of the visible surface crack. In the HyFRC specimens corrosion product deposition was observed in the central region of the bar (area of highest tensile demand during cyclic loading) covering 24% and 28% of the exposed surface area for specimens H2 and H3 respectively.

The digital scans of Fig. 43 were of specimens C2 and H2 and represented the region of greatest damage to the rebar. From a qualitative perspective it is apparent that significantly more damage is visible on the C2 specimen. Note that C2 fractured during post corrosion flexural testing so it becomes difficult to differentiate between necking due to plastic deformation of the bar and section reduction due to localized corrosion at the crack. The remnants of a bar rib are visible across the fracture surface of C2 so it is apparent from a comparison of the surrounding ribs that a significant degree of localized corrosion was in fact happening at the point of fracture. The measured mass loss of the rebar is provided in Table 6 and confirms the electrochemical monitoring results and provides tangible support for corrosion reduction in the presence of the HyFRC for the conditions under examination.

Table 6 – Measured mass loss for corroded rebar

	Specimen			
	C2	C3	H2	H3
Mass Loss [g]	21.3	18.9	7.8	4.0

4.2 Corrosion Propagation Experiments (Cylindrical Specimens)

This section describes the specimens used to examine active corrosion rates once corrosion has initiated. The specimens were characteristic of a lollipop style specimen with a single piece of rebar surrounded by concrete or HyFRC matrix. The entire rebar surface was sandblasted to remove mill scale and one end was drilled and tapped to provide electrical connection through a screw and ring terminal. Bar ends were protected by first applying a layer of 3M brand Skotchkote® moisture sealant, wrapping with electrical tape and then by covering with polyolefin heat shrink tubing. The specimen size and corrosion monitoring cell are shown in Fig. 44.
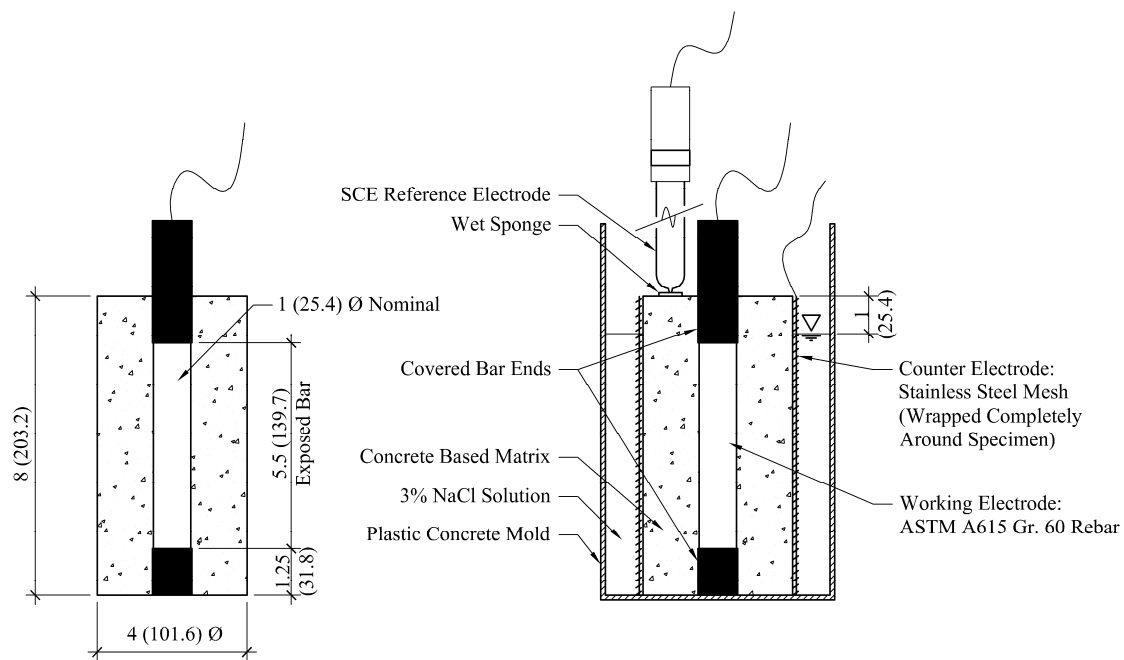
Fig. 44 – Dimensions and corrosion cell for corrosion propagation specimens [inch (mm)]

The specimens were prepared with a type CONC1 matrix (see Table 2) and contained entrained air adjusted between 5-8%. Six specimens were made with a plain concrete matrix and 6 were made with the proposed fiber hybridization. Sodium chloride was

added directly to the mix water as well (4% Cl⁻ based on cement weight) and specimens were stored in the fog room in between monitoring intervals. The addition of the NaCl in this manner was to provide an immediate and equivalent source for corrosion initiation, such that ambiguities associated with the time for Cl⁻ propagation through the matrix cover would be eliminated. During corrosion monitoring periods, specimens were removed from the fog room, wrapped in a stainless steel mesh and placed in a cylindrical container containing a 3% NaCl solution (see Fig. 44).

Corrosion monitoring was carried out as described in section 4.1. The periodic E_{oc} and i_{tot} measurements are provided in Figs. 45 and 46 and the data is reported in the format as described in section 4.1.
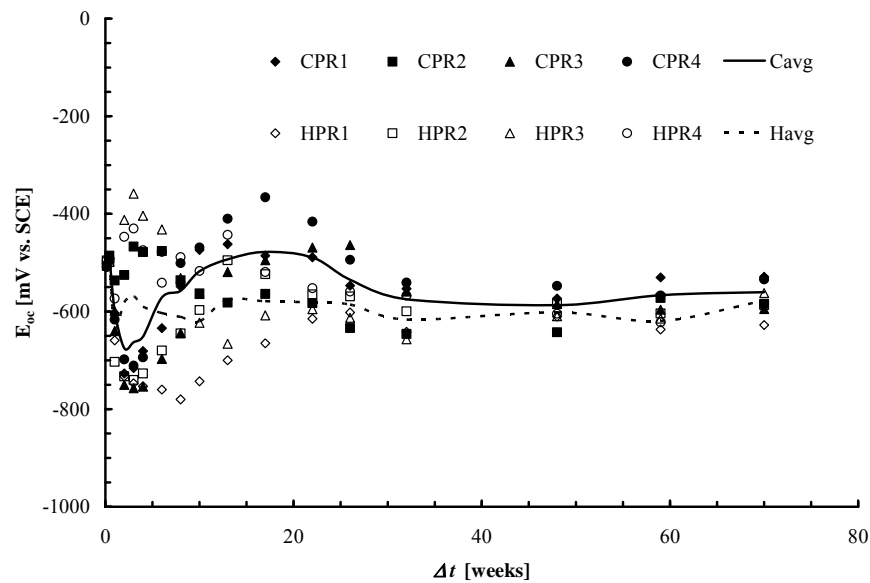
Fig. 45 – Cylindrical specimen corrosion potentials
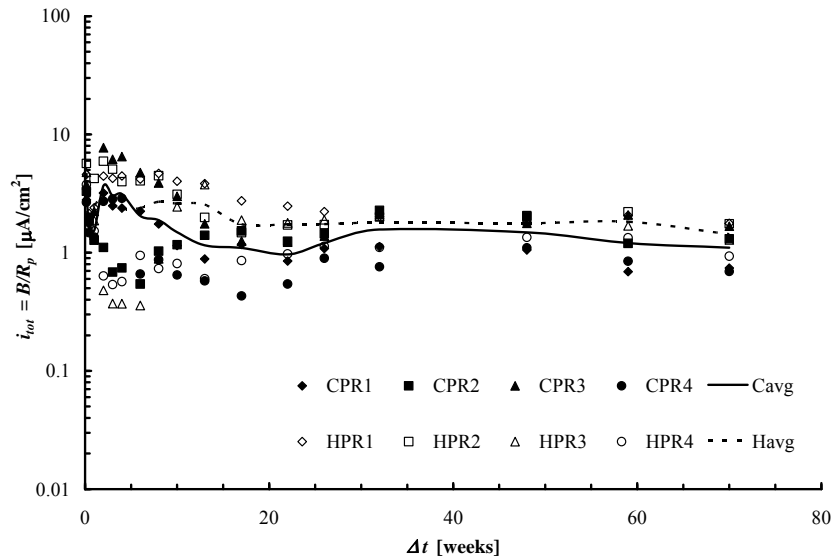
Fig. 46 – Estimated cylindrical specimen corrosion current densities

Comparison of the E_{oc} and i_{tot} behavior shows nearly identical behavior between the "C" type and "H" type specimens. At the conclusion of the 70 week monitoring period, the total average charge transfer was calculated numerically based on the method proposed by (4.4) in section 4.1.3. The total average charge transfer for the "C" and "H" specimens was 6.8×10^9 and 9.0×10^9 coulombs respectively. These values are within the 2x error associated with the assumed value of B so any conclusions regarding variation in the material performance due to the inclusion of fibers are unclear. The most likely explanation was that under the observed corrosion rates the amount of corrosion product formation was not substantial enough to induce cracking at a magnitude that would change the nature of the corrosion reaction between the plain concrete and HyFRC specimens. Corrosion rates were therefore governed by the O_2 concentrations and the ionic conductivity of the bulk concrete based matrix (assumed equivalent for both specimen types).

With respect to this hypothesis, preliminary investigations that used current control show promising results. Two of the cylindrical corrosion propagation specimens were placed in the cell shown in Fig. 44 and a Gamry G 750 potentiostat was used with galvanostatic control to force a 3 mA/cm^2 corrosion current density through the cell. The current flow was periodically interrupted in order to measure the polarization resistance of the specimen. These results are shown in Fig. 47 with a schematic of the state of surface cracking at the conclusion of the test. The data shows the total estimated corrosion current density i_{tot} based on polarization resistance measurements as a function of the total charge transfer Q_{tot} from the impressed current (section 4.1, Eq. 4.4 for Q_{tot} calculation).
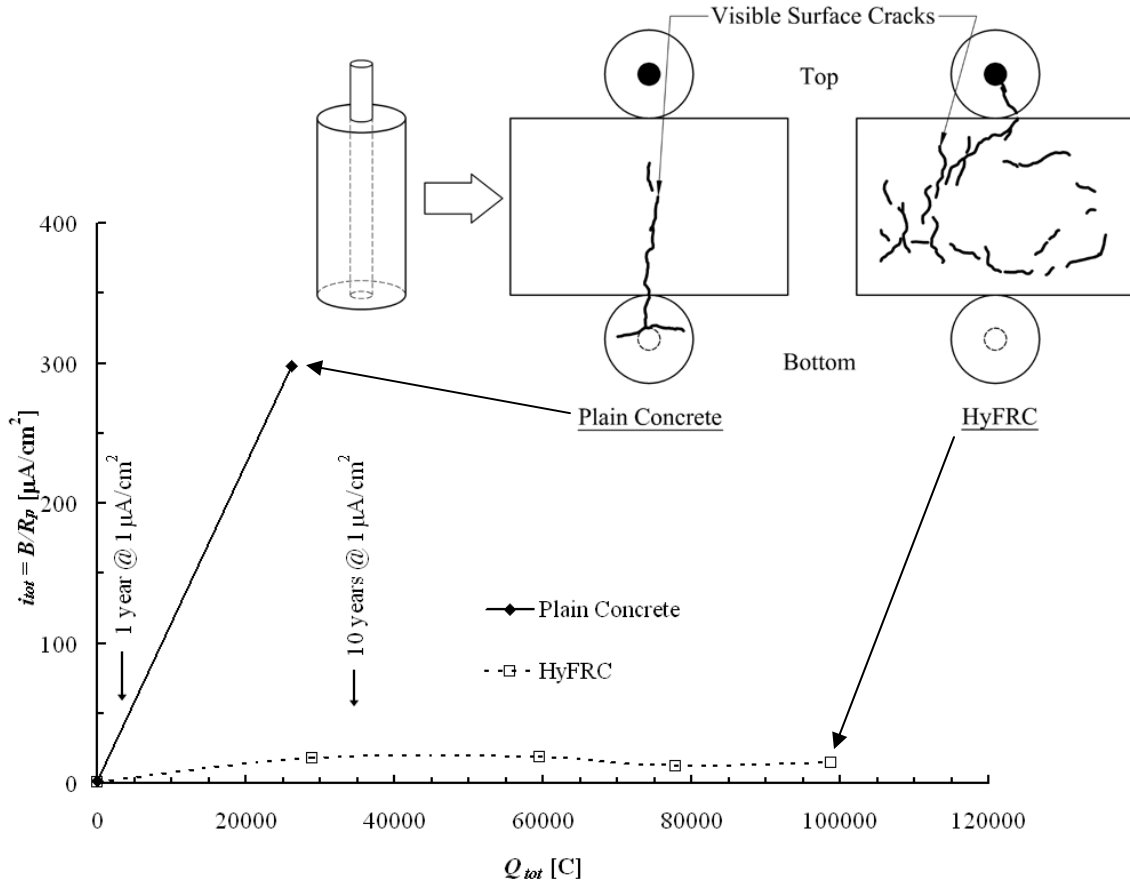
Fig. 47 – Accelerated test results of cylindrical specimens ($B = 26$ mV)

The total accelerated charge transfer was chosen as the basis for comparison because it can be correlated with corrosion product formation. Larger values of Q_{tot} means greater amounts of mass loss at the surface of the rebar. This can be correlated with a larger amount of corrosion product formation, which is the mechanism behind internal expansion and cracking in the concrete.

It was observed within 24 hours of acceleration, the i_{tot} of the plain concrete specimen jumped 2 orders of magnitude from 1.3 μA/cm² to 298 μA/cm². In the same interval the i_{tot} of the HyFRC specimen only increased to 18 μA/cm² (from 1.1 μA/cm²) and persisted

57

at this value for the following 2 days. The degree of acceleration is also represented on

Fig. 47 with markers representing the estimated Q_{tot} based on the magnitude of the

corrosion current density for this specimen. As a point of comparison an $i = 1$ $\mu A/cm^2$

(characteristic value from Fig. 46) corrosion current density would take 8.2 years to reach

the same magnitude of Q_{tot} as 24 hours of $i = 3$ mA/cm^2. The surface cracking was

illustrated as well and provides a significant point of contrast between the two materials.

It is difficult to say at this point in the investigation whether the observed increase in i_{tot}

was due to decreased cell resistance, a greater rate of O_2 diffusion to the bar surface, a

greater area of depassivation or some combination of these mechanisms, however one

can confidently conclude that the degree of cracking has a considerable influence on all

these factors. The plain concrete specimen developed a single dominant crack parallel to

the rebar that branched at the base in manner characteristic of spalling, while the HyFRC

specimen developed a network of multiple cracks that spread over the entire surface. It is

noted that the crack surface figures represent the state of the material at the conclusion of

acceleration such that the cracking in the HyFRC is due to nearly 4x as much charge

transfer when compared to the plain concrete. Had the degree of surface cracking been

mapped at equivalent amounts of Q_{tot}, then it is likely that the appearance of surface

cracking in the HyFRC would have been less pronounced.

4.3 Freeze-Thaw

The following sections summarize the results of the freeze-thaw validation study conducted on the plain concrete and the HyFRC materials. It is emphasized that these experiments were necessary because the HyFRC material was designed for Area III requirements, such that demands associated with freeze-thaw were to be expected. Validation was carried out by performing both accelerated freeze-thaw and surface salt scaling tests.

4.3.1 Cyclic Freeze-Thaw

Accelerated freeze-thaw tests were carried out per ASTM C666, procedure A using a Humboldt® freeze-thaw cabinet (model number H-3185SD). Three prismatic specimens with dimensions of 3.5 x 4.5 x 16 in. (89 x 114 x 406 mm) were prepared for each material type using a CONC1 matrix with air entraining adjusted between 5-8%. The plain concrete specimens have the designations C1, C2 and C3 while the HyFRC use H1, H2 and H3. Although similar, these designations do not represent the specimens that were previously reported in section 4.1.3. Following casting, specimens were wet cured in a fog room for 14 days before placement in the freeze-thaw cabinet and the start of cycling. Four air entrained, plain concrete specimens were also prepared with an embedded type T thermocouple in order to provide a means to measure the temperature in the center of the specimen. These temperature monitoring specimens were spaced throughout the freeze-thaw cabinet in order to characterize temperature variations at different positions within the cabinet. An example of the relative variation in temperature for the four specimens through 3 freeze-thaw cycles is provided in Fig. 48.
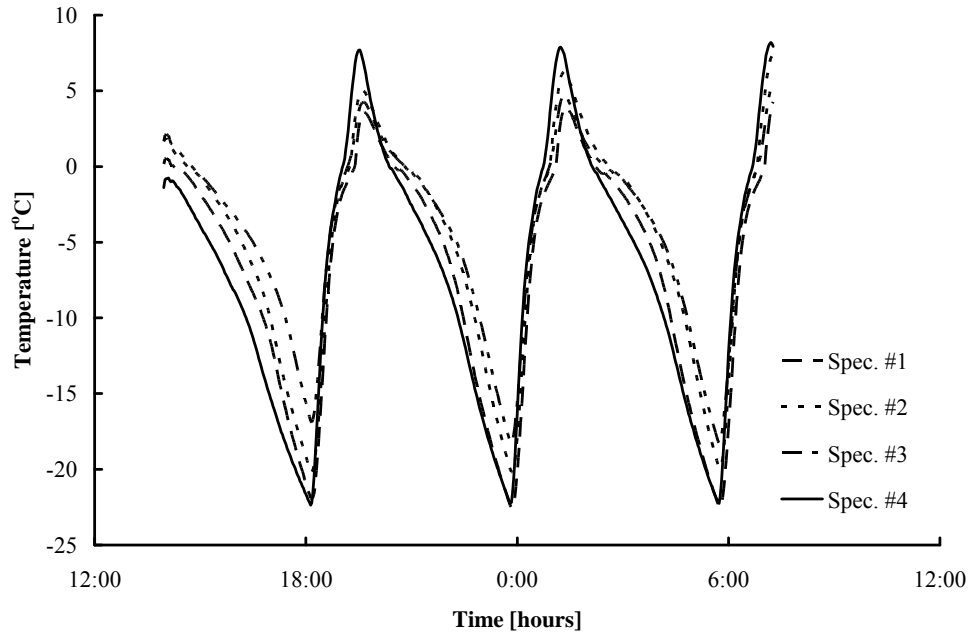
Fig. 48 – Example temperature variation within the freeze-thaw specimens

It was apparent that a slight variation existed within the cabinet, so all the specimens were rotated through the different positions after the weekly monitoring sessions. Damage in the specimens was monitored both quantitatively using ASTM C215 (fundamental longitudinal frequency) and qualitatively by examining the exterior surface at the conclusion of testing. In order to calculate the dynamic modulus E_D of the specimen from the fundamental longitudinal frequency, the material density was needed. This was calculated in accordance with ASTM C138 and the values are provided in Table 7.

Table 7 – Physical properties of the freeze-thaw specimens

Specimen	Air Content [%]	Density [lb/ft^3 (kg/m^3)]
H1	5.2	146.2 (2342)
H2	5.3	146.1 (2340)
H3	5.1	146.4 (2345)
H$_{avg}$	5.2	146.2 (2342)
C1	5.8	141.3 (2263)
C2	6.1	140.8 (2256)
C3	6.0	140.9 (2257)
C$_{avg}$	6.9	141.0 (2259)

With values of the specimen density ρ, E_D could then be calculated directly from the measurements of the fundamental longitudinal frequency. This relationship is as follows

$$E_D = 4n^2 L^2 \rho \cdot 10^{-12} \text{ [MPa]} \tag{4.5}$$

where n is the fundamental longitudinal frequency [Hz], L is the specimen length [mm] and ρ is the specimen density [kg/m^3]. The specimen length L was measured at 16 in. (406 mm) for all specimens. The variation in E_D as a function of the number of freeze-thaw cycles is provided in Fig. 49. Data is shown in similar fashion to the corrosion results where the discrete data points are provided with an idealized continuous average.
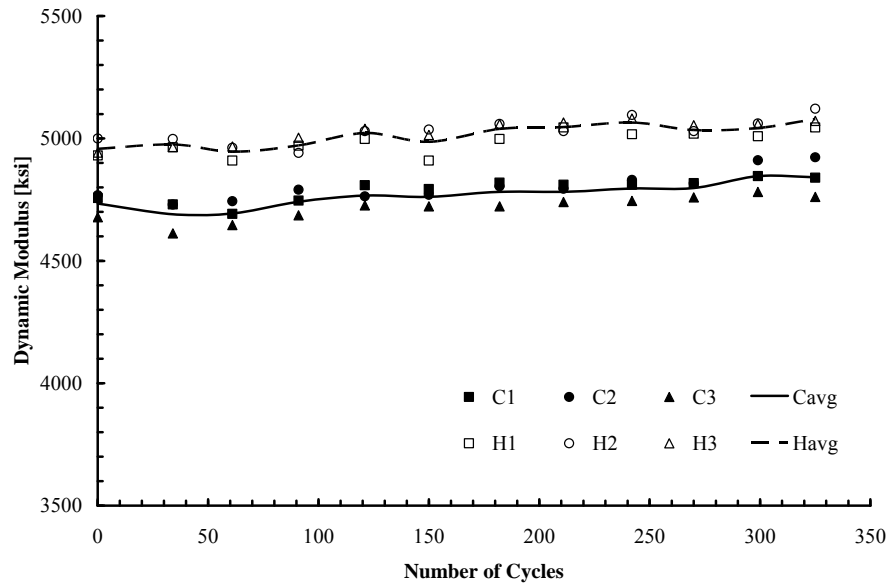
Fig. 49 – Dynamic modulus E_D variation with freeze-thaw cycling [multiply by 6.89×10^{-3} for GPa]

Throughout the freeze-thaw cycling both the HyFRC and plain concrete specimens showed increases in E_D. Average increases for the HyFRC were on the order of 2.4% (from 4958 (34.2) to 5079 ksi (35.0MPa)) and the plain concrete showed increases on the order of 2.3% (from 4734 (32.6) to 4841 ksi (33.4 MPa)). The increase can be attributed to continued hydration due to the fact that freeze thaw cycling was started after only 14 days of wet curing and the specimens remained in a saturated state during the three month test period. The lack of material degradation demonstrates the adequacy of the air void system for both specimen types. At the conclusion of the experiment, specimens showed noticeable surface scaling (Fig. 50). The larger amount of exposed aggregate on the surface of the plain concrete specimens represents a higher degree of surface mortar scaling and a corresponding loss in specimen mass.

62

Fig. 50 – Freeze-thaw specimen surface (a) before, (b) plain concrete after and (c) HyFRC after freeze-thaw cycling

4.3.2 Surface Scaling Resistance

Scaling specimens were prepared and tested in accordance with ASTM C672. Slab specimens 10 x 10 x 3.5 in. (254 x 254 x 89 mm) were cast and PVC ponding dams were adhered to the top surface. Five specimens were cast for each mix. A 4% $CaCl_2$ solution was ponded on the top surface and the specimens were placed in an environmentally controlled freezing chamber (-10 ^{o}C) for 18 hours with the remaining 6 hours of a day spent thawing in the ambient lab environment. This cycle continued through the regular

work week and the specimens were kept frozen over the weekend. At the end of multiples of 5 cycles, specimen surfaces were flushed and photographed for condition assessment. The ASTM standard provides a guide for surface assessment which can be summarized as follows:

- Rating = 0:   no scaling
- Rating = 1:   very light scaling (1/8" max depth & no coarse aggregate visible)
- Rating = 2:   slight to moderate scaling
- Rating = 3:   moderate scaling (some coarse aggregate visible)
- Rating = 4:   moderate to severe scaling
- Rating = 5:   severe scaling (coarse aggregate visible over the entire surface).

The rating system is subjective in nature, however accompanied by photographs it can provide a relative measure of the degree of scaling between multiple types of specimens, coating systems, curing methods, etc. A summary of the surface condition assessment through 50 cycles is provided in Table 8 along with a picture of the specimen surface prior to ponding (Fig. 51) and all specimens after ponding (Figs. 52 and 53).

Table 8 – Scaling specimen surface ratings and cumulative values

Number	Plain Concrete					HyFRC				
of Cycles	C1	C2	C3	C4	C5	H1	H2	H3	H4	H5
0	0	0	0	0	0	0	0	0	0	0
5	2	1	1	1	1	1	0	0	0	1
10	3	2	2	1	2	1	0	0	1	1
15	3	2	2	1	2	1	0	1	1	1
20	3	2	2	2	2	1	0	1	1	1
25	3	2	2	2	2	1	0	1	1	1
50	3	2	2	2	2	1	0	1	1	2
Σ	17	11	11	9	11	6	0	4	5	7
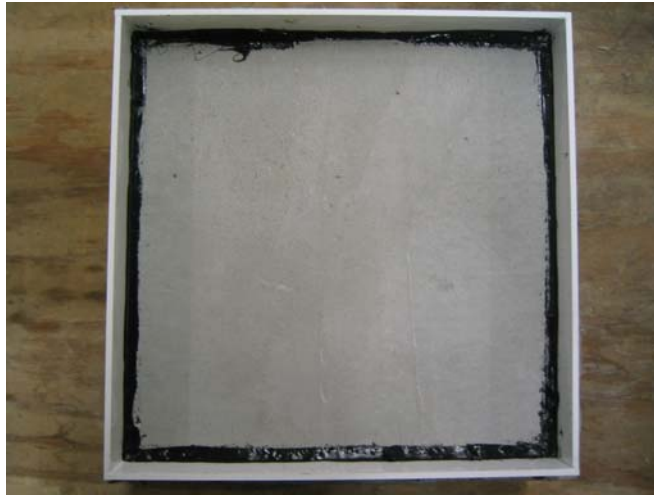
F

Fig. 51 – Surface condition before salt scaling (specimen C1)
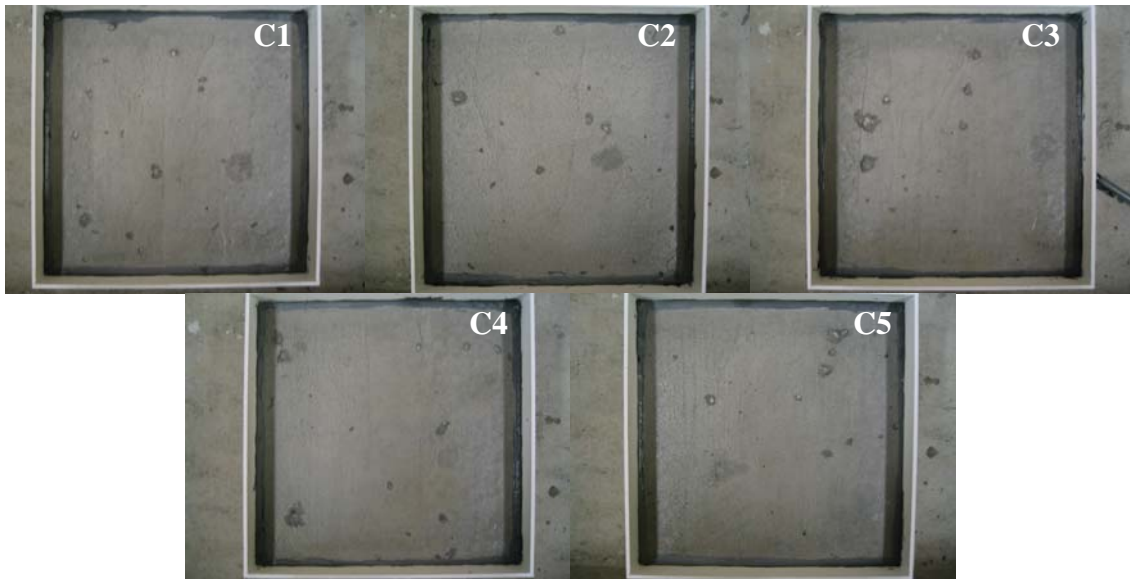
Fig. 52 – Surface condition of plain concrete specimens following 50 cycles of salt scaling
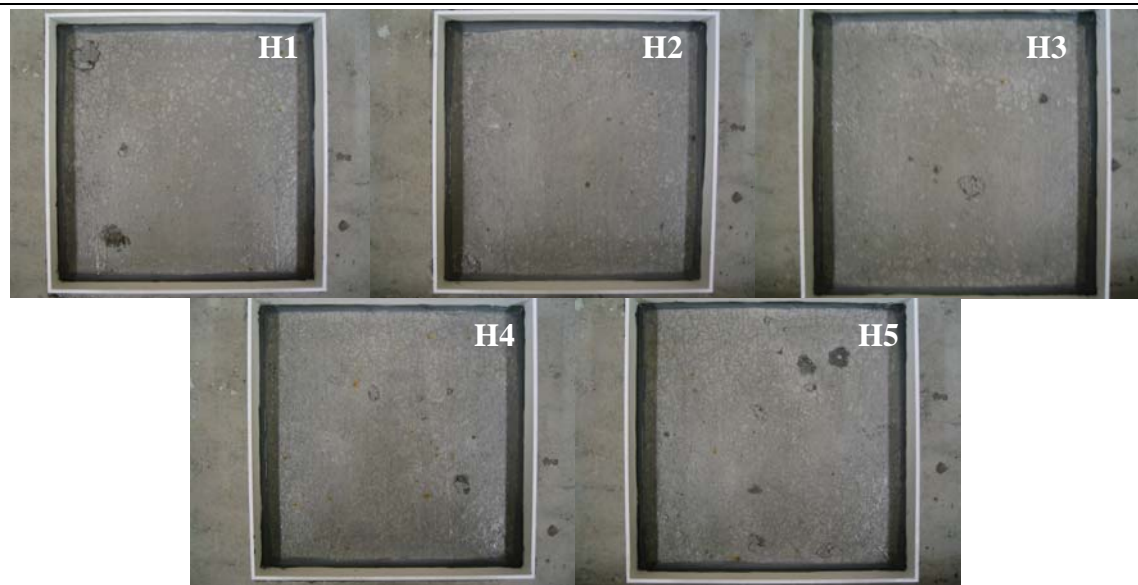
Fig. 53 – Surface condition of HyFRC specimens following 50 cycles of salt scaling

The cumulative values at the bottom of Table 8 are representative of the time-history behavior of the specimens. Higher values signify that the specimens reached higher degrees of scaling earlier. The fact that the cumulative scaling value of the control specimens is nearly double the HyFRC highlights the microfiber's ability to impact surface level interactions. Their small size and high numerical density make the microfibers ideal to resist microcrack propagation associated with the expansive mechanisms of salt based scaling. This observation is supported by the fact that others (Debatin 2008) have observed enhanced spalling resistance to freeze-thaw damage in the presence of PVA microfibers as well.

5 SELF CONSOLIDATING MIX DESIGN

During the course of the HyFRC development and testing program, concern was given to the workability of the mix. Addition of the fibers created a no slump mix which required significant amounts of external vibration in order to properly consolidate. In order to facilitate the availability of the HyFRC to a wider range of applications, workability had to be improved in order to ensure pumpability and a higher degree of consolidation under the material's own flow. For this reason, a preliminary investigation was conducted that experimented with a self consolidating concrete (SCC) mix design.

The admixture suite consisted of a polycarboxylate superplasticizer (Glenium 3030) and an organic viscosity modifying agent (Rheomac VMA 358). Both products are produced by BASF admixtures. In order to promote higher levels of material consistency and flowability, significant changes were also made to the mix designs already discussed (see Table 2). The total cementitious material content was increased to 900 lb/yd^3 (534 kg/m^3). An ASTM C618 Type C fly ash was introduced at 25% by weight of the total cementitious content in order to reduce the overall cement demand to 675 lb/yd^3 (400 kg/m^3). The water to cementitous material content was increased to 0.45. The same pea gravel and sand were used as previously described, but the S/G proportions were increased to 2.0. These SCC mix proportions are summarized in Table 9.

Table 9 – Relative mix proportions for a self consolidating HyFRC

Cement[a]	Fly Ash[b]	Water	CA[c]	FA[d]	Super[e]	VMA[e]	Fiber Dosage V_f [%]		
							PA	S1	S2
1.0	0.33	0.6	1.24	2.45	0.0012	0.0003	0.2	0.5	0.8

[a] ASTM C150 Type II
[b] ASTM C618 Type C
[c] pea gravel, 3/8 in. MSA
[d] coarse sand, FM = 3.2
[e] value shown as the weight of solids content

With the use of this mix, a conventional slump cone (ASTM C143) could be used to characterize the mix consistency and a value of 6.5 in. (165 mm) was obtained. The flexural performance of the mix was characterized by casting beam specimens with the dimensions shown previously (Fig. 6). It must be emphasized that the beams were cast by placing the mix directly into the molds without external vibration. Specimens were cured in the aggressive environment (7 day wet followed by 21 day dry) and then tested in four point bending. These results are shown in Fig. 54.
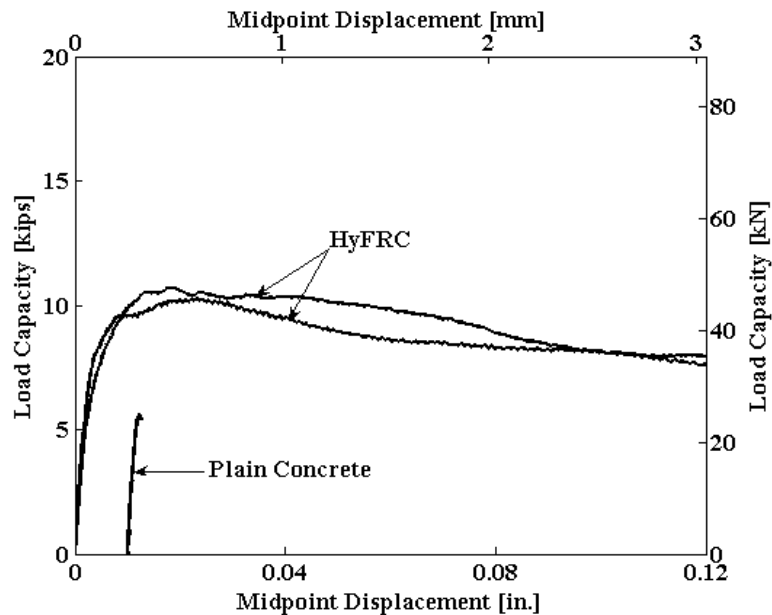
Fig. 54 – SCC flexure tests (plain concrete shifted from origin for clarity)

The characteristic increases in both material flexural strength and toughness were still observed, which implies higher levels of crack resistance previously noted in the durability studies. It must be noted however, that this SCC mix was not the one used during the durability characterization portion of the study, so generalizations regarding its performance under aggressive environments should be approached with caution until validation studies can be performed.

6   RECOMMENDATIONS FOR OPTIMAL IMPLEMENTATION

In section 2, it was observed that the use of a deflection hardening HyFRC composite can result in increased flexural strength and stiffness. These increases are significant enough to warrant further study on how the element could be redesigned to optimize performance in terms of costs. Researchers have already used the beneficial properties of various fiber reinforced composites to reduce the amount of rebar in bridge decks (Kim et al. 2004, Naaman and Chandrangsu 2004). This being said, the enhanced post crack strength and stiffness provided by the HyFRC has some interesting implications for element design. Examination of the average EDP's from Table 3 demonstrates that the flexural response of a HyFRC element is stiffer and stronger than a reinforced concrete element with a low reinforcing ratio (ρ_s = 0.3%) up to the point of rebar yield. Low reinforcing ratios are typically used when demands on the element are based on shrinkage and temperature fluctuations that induce tensile strains at or above the cracking limit of the plain concrete. The enhanced flexural behavior of the HyFRC implies that it may be an adequate substitute for the rebar (when used at low ρ_s), thereby virtually eliminating the means for corrosion based deterioration of the structure.

Methods for optimum element design can be carried out in one of two ways; (1) reductions in existing element reinforcing ratios ρ_s or (2) reductions in element thickness due to enhanced post crack flexural stiffness. For example, consider the typical detail for a Type R(9S) bridge approach slab as shown in Fig. 55.

70
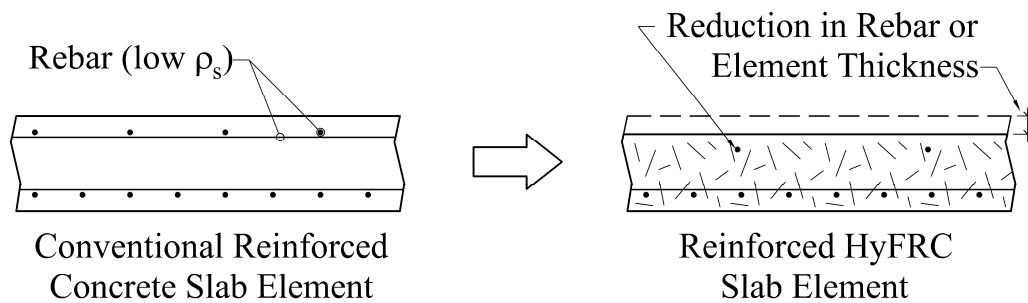
Fig. 55 – Proposed methods for optimum element design using HyFRC flexure properties

It is assumed that the original design intent is to resist one-way strong direction bending such that only the bottom surface experiences significant tension. For this reason a relatively large ρ_s is used at the bottom, while a lower ρ_s is used at the top in order to resist minor cracking associated with shrinkage and temperature related strains. From the data presented in Table 3 and Fig. 13, it is evident that for certain element thicknesses and ρ_s, plain HyFRC is expected to be stronger and stiffer than reinforced concrete. Under these circumstances the top steel could be eliminated if the slab is composed of HyFRC. Consideration of the data presented in Fig. 14 shows that HyFRC in combination with larger reinforcing ratios ($\rho_s = 1.1\%$), results in stiffer and stronger flexural responses. For this reason it may be possible to decrease the element thickness when service level loads result in post crack flexural demands, which would result in lower amounts of material use.

One concern that may arise is how the removal of a layer of rebar (albeit, a relatively small amount) will affect the compression ductility of the element. Rebar is typically used in the flexural compression region of an element (the top layer in this example) in

order to increase flexural ductility. Studies done by RILEM (1977) and Campione (2002) have demonstrated that the presence of fibers creates an effective confinement in the compression region, which increases the composite's overall compression ductility. The ductility enhancement created by the fibers may be enough to compensate for any reductions created by rebar removal. Of course it must be noted that the general outline for element design using HyFRC in this example should be treated on an application by application basis. Scaling effects associated with the material flexural behavior (Stang 2003) must be noted as well as the amount of rebar considered for removal. Ideally full scale tests should be implemented in order to verify the element performance.

7   SUMMARY AND CONCLUSIONS

The research program consisted of four parts. In Part I a performance based materials approach to bridge approach slabs was developed. The fiber reinforced composite was designed to exhibit deflection hardening through an average measure of ductility exceeding the yield strain of steel rebar (i.e. > 0.002). Four point flexure tests on 6 in. (152 mm) deep beam specimens were conducted in order to quantify the material flexure performance.

In Part II, the existing California Department of Transportation (CalTrans) bridge approach slab design was used as the basis for element sizing and reinforcement ratios. Four-point flexure tests (1/2 scale models of an existing bridge approach slabs) were conducted and HyFRC beams were compared against plain concrete control beams with and without conventional steel reinforcement. For the beam elements under examination the use of the deflection hardening HyFRC mix design proposed in this study resulted in increases in flexural strength and stiffness (relative to a plain concrete based matrix) for rebar reinforcing ratios as high as 1.1%.

In Part III an extensive durability study was conducted on how the crack resistance provided by the HyFRC mitigates durability problems associated with frost action and corrosion. The bridge approach slab is highly susceptible to deterioration from freeze-thaw cycling and reinforcement corrosion due to the anticipated location (i.e. Area III jurisdiction). Compared to the plain concrete specimens the HyFRC exhibited improved

performance in regards to both freeze/thaw resistance and scaling resistance. To study the effect of cracking/crack resistance on corrosion behavior, cyclic flexure tests were conducted on reinforced beam elements composed of HyFRC and a comparable plain concrete in order to induce surface cracking. For a specified load demand in excess of the plain concrete f_r and below the yield strength of the rebar, the HyFRC flexural specimens showed a high propensity for crack resistance (no surface cracks were visible as opposed to the reinforced plain concrete).

Corrosion behavior was monitored by ponding salt solution on the cracked surface and higher corrosion rates i_{corr} (measured by polarization resistance) by nearly 1 order magnitude were observed in the reinforced plain concrete specimens. The observed increased corrosion rates were confirmed by direct gravimetric analysis of the bars after removal.

The crack resistance provided by the fibers can influence the corrosion initiation behavior of embedded rebar in beam elements cracked by flexural loading. This phenomenon was observed under equivalent flexural load based demands which exceeded the plain concrete matrix modulus of rupture, but were less than the point of rebar yield. Preliminary investigation with accelerated corrosion in cylindrical specimens shows that crack resistance can also reduce corrosion rates late in the life of the element when corrosion pressures at the rebar/matrix interface are significant enough to induce cracking and bond loss.

In Part IV the study concludes with a discussion of how the observed improvements in flexural performance in the presence of the fibers can be used for a new design detail for bridge approach slabs. The improved mechanical performance may have implications for the design of certain structural elements (such as section or rebar reduction), however it is anticipated that scaling effects will become apparent at large displacement demands when the HyFRC begins to soften. It is anticipated that performance increases (i.e. increased crack resistance, flexural stiffness and strength) will be observed when the HyFRC is used in place of plain concrete, however the exact magnitude should be verified with full scale testing. In the case of element redesign (i.e. section or rebar reduction) full scale testing is highly recommended.

Investigation into the use of self-consolidating admixtures verified that it is possible to produce a mix design with the hybrid fiber gradation that can consolidate under its own flow (no external vibration was necessary). The self consolidating mix design provided in this study is not proposed as an optimum, rather it is a proof of concept based on trial batching that will require further work in order to verify the optimum admixture content (i.e. minimum superplasticizer and viscosity modifier that produces the necessary level of consistency). Further work can also be done to adapt the hybrid fiber gradation to an early strength version that can be used as a highly durable rapid curing repair/rehabilitation material.

8 IMPLICATION OF HyFRC FOR FIELD APPLICATIONS

The HyFRC developed for CalTrans for the use in bridge approach slabs meets the necessary material performance criteria. The concept stage and laboratory prototype stage have been completed to date. The next and final stage needs to focus on successful implementation of HyFRC for cast-in-place application of bridge approach slabs.

Other concrete structures such as for example bridge decks have similar material performance criteria (i.e. need to be crack resistant and durable) in order to increase their service life, minimize repair, maintenance, and disruption to traffic flow. Hence, the HyFRC will exhibit superior performance in these applications as well.

REFERENCES

ACI 318, (2002). "Section 4.2.2," *Building Code Requirements for Structural Concrete*, American Concrete Institute, Farmington Hills, Michigan.

ACI 544.1R-96, (1997), Section 4.2, *State of the Art Report on Fiber Reinforced Concrete*, American Concrete Institute, Farmington Hills, Michigan.

Al-Tayyib, A. and Al-Zahrani, M., (1990). "Corrosion of Steel Reinforcement in Polypropylene Fiber Reinforced Concrete Structures," *ACI Materials Journal*, 87(2), 108-113.

Andrade, C. and Gonzalez, J., (1978). "Quantitative Measurements of Corrosion Rate of Reinforcing Steels Embedded in Concrete Using Polarization Resistance Measurements," *Werkstoffe und Korrosion*, 29, 515-519.

Andrade, C. and Alonso, C., (1996). "Corrosion Rate Monitoring in the Laboratory and On-Site," *Construction and Building Materials*, 10(5), 315-328.

Banthia, N. and Trottier, J.F., (1995). "Test Methods for Flexural Toughness Characterization of Fiber Reinforced Concrete: Some Concerns and a Proposition," *ACI Materials Journal*, 92(1), 48-57.

CalTrans, (2003). "Section 8.22, Protection Against Corrosion," *CalTrans Bridge Design Specifications,* California Department of Transportation.

Campione, G., (2002), "The Effects of Fibers on the Confinement Models for Concrete Columns," *Canadian Journal of Civil Engineering*, 29, 742-750.

Cheyrezy, M., Daniel, J.I., Krenchel, H., Mihashi, H., Pera, J., Rossi, P. and Xi, Y., (1995), "Specific Production and Manufacturing Issues," *High Performance Fiber Reinforced Cement Composites – HPFRCC2*, Naaman, A.E. and Reinhardt, H.W. eds., Ann Arbor, USA, 25-42.

Debatin, J., (2008). *Effect of Fibers on Damage Mitigation Due to Frost Action*, Bachelor's thesis, University of California, Berkeley.

Johnson, P., Couture, A., and Nicolet, R., (2007). *Commision of Inquiry into the Collapse of a Portion of the de la Concorde Overpass*, Commission d'enquete sur le viaduc de la Concorde; Library and Archives Canada.

Kim, Y., Fischer, G. and Li, V.C., (2004), "Performance of Bridge Deck Link Slabs Designed with Ductile Engineered Cementitious Composite," *ACI Structural Journal*, 101 (6), 792-801.

Kyle, N., (2001), *Subsidence Cracking of Concrete Over Steel Reinforcement Bar in Bridge Decks*, M.S. Thesis, Virginia Polytechnic Institute and State University, Blacksburg, Virginia.

Laplante, P., Aitcin, P.C. and Vezina, D., (1991). "Abrasion Resistance of Concrete", *Journal of Materials in Civil Engineering*, 3(1), 19-28.

Li, V.C. and Wu, H.C., (1992). "Conditions for Pseudo Strain-Hardening in Fiber Reinforced Brittle Matrix Composites," *Journal of Applied Mechanics Review*, 45(8), 390-398.

Li, V.C., Wang, S. and Wu, C., (2001), "Tensile Strain-Hardening Behavior of Polyvinyl Alcohol Engineered Cementitious Composite (PVA-ECC)," *ACI Materials Journal*, 98 (6), 483-492.

Mangat, P.S. and Swamy, R.N., (1974a), "Compactibility of Steel Fibre Reinforced Concrete," *Concrete*, 8 (5), 34-35.

Mangat, P.S., and Swamy, R.N., (1974b), "Influence of Fibre-Aggregate Interaction on some Properties of Steel Fibre Reinforced Concrete," *Materials and Structures*, 7 (41), 307-314.

Massicotte, B., Degrange, G. and Dzeletovic, N., (2000), "Mix Design for SFRC Bridge Deck Construction," *5th RILEM Symposium on Fibre-Reinforced Concretes (FRC)*, Rossi, P. and Chanvillard, G. eds., Lyon, France, 119-128.

Naaman, A.E., (2003). "Strain Hardening and Deflection Hardening Fiber Reinforced Cement Composites." *In: Naaman, A.E. and Reinhardt, H.W. eds. High Performance Fiber Reinforced Cement Composites (HPFRCC4)*, 95-113.

Naaman, A.E. and Chandrangsu, K., (2004), "Innovative Bridge Deck System Using High-Performance Fiber-Reinforced Cement Composites," *ACI Structural Journal*, 101 (1), 57-64.

RILEM Technical Committee 19-FRC, (1977), "Fibre Concrete Materials," *Materials and Structures*, 10 (56), 103-120.

Rossi, P., Acker, P., and Malier, Y., (1987), "Effect of Steel Fibres at Two Different Stages: the Material and the Structure," *Materials and Structures*, 20, 436-439.

Rossi, P. and Harrouche, N., (1990), "Mix Design and Mechanical Behaviour of some Steel-Fibre-Reinforced Concretes used in Reinforced Concrete Structures," *Materials and Structures*, 23, 256-266.

Rossi, P., (2001). "Utlra-High-Performance Fiber-Reinforced Concretes," *Concrete International*, 23(12), 46-52.

Seo, J., Ha, H., and Briaud, J.L., (2002). "Investigation of Settlement at Bridge Approach Slab Expansion Joint: Numerical Simulations and Model Tests," Report No. FHWA/TX-03/0-4147-2, Texas Department of Transportation.

Stang, H., (2003). "Scale Effects in FRC and HPFRCC Structural Elements." *In: Naaman, A.E. and Reinhardt, H.W. eds. High Performance Fiber Reinforced Cement Composites (HPFRCC4)*, 245-258.

Tepfers, R., (1979). "Cracking of Concrete Cover Along Anchored Deformed Reinforcing Bars," *Magazine of Concrete Research*, 31(106), 3-12.

Timmerman, D.H., (1976). "An Evaluation of Bridge Approach Design and Construction Techniques," Report No. OHIO-DOT-03-77, Ohio Department of Transportation.

Tjiptobroto, P. and Hansen, W., (1993). "Tensile Strain Hardening and Multiple Cracking in High-Performance Cement-Based Composites Containing Discontinuous Fibers," *ACI Materials Journal*, 90(1), 16-25.

White, D., Sritharan, S., Suleiman, M., Mekkawy, M. and Chetlur, S., (2005). "Identification of the Best Practices for Design, Construction, and Repair of Bridge Approaches," Report No. CTRE Project 02-118, Iowa Highway Research Board.

Wood, J., (2008). "Implications of the Collapse of the de la Concorde Overpass," *Structural Engineer*, 86 (1), 16-18.